

12

AD A113673



CR 82.013

**NAVAL CIVIL ENGINEERING LABORATORY
Port Hueneme, CA**

**Sponsored by
NAVAL FACILITIES ENGINEERING COMMAND**

**A VERIFICATION STUDY FOR THE BOUNDING SURFACE
PLASTICITY MODEL FOR COHESIVE SOILS**

March 1982

An Investigation Conducted by
Department of Civil Engineering
University of California, Davis
Davis, CA

N62583-81-MR-320

DTIC
APR 21 1982
SSD
H
[Handwritten signature]

Approved for public release; distribution unlimited

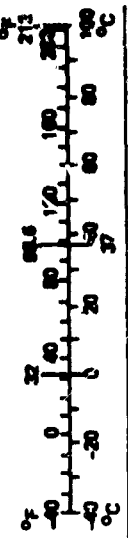
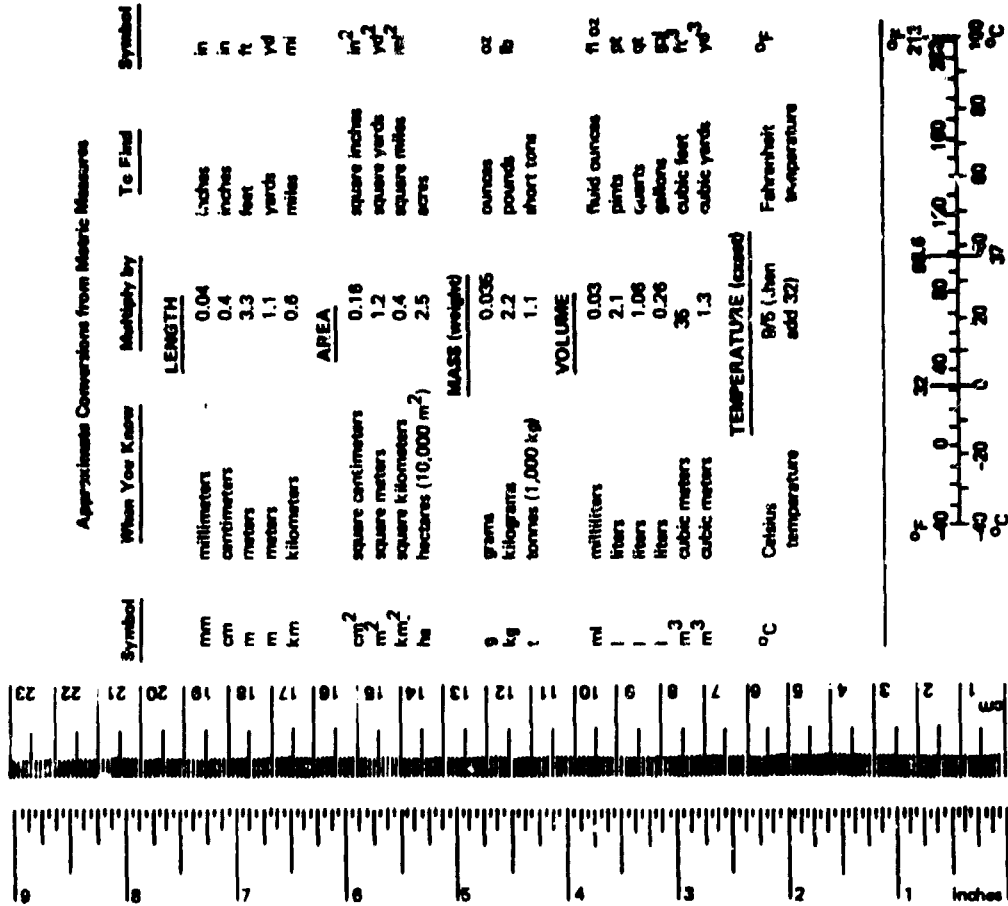
82 04 21 04Z

DTIC FILE COPY

METRIC CONVERSION FACTORS

Approximate Conversions to Metric Measures				Approximate Conversions from Metric Measures			
Symbol	When You Know	Multiply by	To Find	Symbol	When You Know	Multiply by	To Find
in ft yd mi	inches feet yards miles	2.5 30 0.9 1.6	centimeters	mm	millimeters	0.04	inches
			centimeters	cm	centimeters	0.4	inches
			meters	m	meters	3.3	feet
in ² ft ² yd ² mi ²	square inches square feet square yards square miles acres	6.5 0.09 0.8 2.6 0.4	kilometers	km	meters	1.1	yards
			square centimeters	cm ²	kilometers	0.6	miles
			square meters	m ²	square centimeters	0.16	square inches
oz lb	pounds short tons (2,000 lb)	28 0.45 0.9	square meters	m ²	square meters	1.2	square yards
			square kilometers	km ²	square kilometers	0.4	square miles
			hectares	ha	hectares (10,000 m ²)	2.5	acres
oz lb	grams kilograms tonnes (1,000 kg)	0.035 2.2 1.1	grams	g	grams	0.035	ounces
			kilograms	kg	kilograms	2.2	pounds
			tonnes	t	tonnes (1,000 kg)	1.1	short tons
tsp Tbsp fl oz c pt qt gal cu ft yd ³	teaspoons tablespoons fluid ounces cups pints quarts gallons cubic feet cubic yards	5 15 30 0.24 0.47 0.96 3.8 0.03 0.76	milliliters	ml	milliliters	0.03	fluid ounces
			milliliters	ml	liters	2.1	pints
			milliliters	ml	liters	1.06	quarts
°F	Fahrenheit temperature	5/9 (after subtracting 32)	liters	l	liters	0.26	gallons
			liters	l	cubic meters	36	cubic feet
			cubic meters	m ³	cubic meters	1.3	cubic yards
TEMPERATURE (exact)			TEMPERATURE (exact)			TEMPERATURE	
						°F	
						Fahrenheit	
						temperature	

*1 in = 2.54 (exactly). For other exact conversions and more detailed tables, see NBS Misc. Publ. 286, Units of Weights and Measures, Price \$2.25, SD Catalog No. C13.10-286.



12

Unclassified

SECURITY CLASSIFICATION OF THIS PAGE (When Data Entered)		READ INSTRUCTIONS BEFORE COMPLETING FORM	
REPORT DOCUMENTATION NUMBER		RECIPIENT'S CATALOG NUMBER	
1 REPORT NUMBER CR 82.013		73	
4 TITLE (and Subtitle) A Verification Study for the Bounding Surface Plasticity Model for Cohesive Soils		5 TYPE OF REPORT AND PERIOD COVERED Final; Feb 1981 - Jan 1982	
7 AUTHOR(s) L. R. Herrmann, C. K. Shen, S. Jafroudi, J. S. DeNatale, and Y. F. Dafalias		8 CONTRACT OR GRANT NUMBER(s) N62583-81-MR-320	
9 PERFORMING ORGANIZATION NAME AND ADDRESS Department of Civil Engineering University of California, Davis Davis, CA 95616		10 PROGRAM ELEMENT, PROJECT, TASK AREA & WORK UNIT NUMBERS YF023.03.01.002	
11 CONTROLLING OFFICE NAME AND ADDRESS Naval Civil Engineering Laboratory Port Hueneme, CA 93043		12 REPORT DATE March 1982	
		13 NUMBER OF PAGES 55	
14 MONITORING AGENCY NAME & ADDRESS (if different from Controlling Office)		15 SECURITY CLASS (of this report) Unclassified	
		15a DECLASSIFICATION DOWNGRADING SCHEDULE	
16 DISTRIBUTION STATEMENT (of this Report) Approved for public release; distribution unlimited			
17 DISTRIBUTION STATEMENT (of the abstract entered in Block 20, if different from Report)			
18 SUPPLEMENTARY NOTES			
19 KEY WORDS (Continue on reverse side if necessary and identify by block number) Soil constitutive model, Finite element, Plasticity, Geotechnical engineering			
20 ABSTRACT (Continue on reverse side if necessary and identify by block number) Results of drained and undrained, triaxial compression and extension, and thick-walled cylinder laboratory tests are given for a laboratory prepared kaolin soil. For the soil in question, a portion of the data is used to calibrate a "bounding surface plasticity model" for cohesive soils. The model is used to analyze the remaining tests and the results are compared to the measured values with good agreement.			

SDTIC
SELECTED
APR 21 1982
H



Accession For	<input type="checkbox"/>
NTIS GRA&I	<input type="checkbox"/>
DTIC TAB	<input type="checkbox"/>
Unannounced	
Justification	
By	
Distribution/	
Availability Codes	
Avail. and/or	
Special	
Dist	

1. Introduction

The work done under the present contract is one phase of an ongoing comprehensive research program at the University of California, Davis Campus, to develop a general constitutive equation for cohesive soils. The ultimate goal of the project is the formulation of reliable, accurate and economical finite element analysis programs for the structural analysis of major geotechnical earth structures. It is anticipated that such analyses will represent a significant advancement over currently available analyses which are based upon less comprehensive representations of soil behavior. The availability of these advanced analysis procedures will significantly enhance our ability to design safer and more economical geotechnical earth structures.

In total the overall project is to consist of five phases: i) theoretical formulation of a comprehensive constitutive model (stress history-strain history relationships) for cohesive soils, ii) validation of the constitutive model by comparing predicted and measured laboratory results for relatively simple experiments, iii) formulation of a systematic procedure for calibrating the model (selecting numerical values for the model parameters for given cohesive soils), iv) numerical implementation of the model so that it can be incorporated into new and existing finite element programs for geotechnical engineering problems and v) demonstration, by comparison of predicted and measured responses of field or model earth structures, of the achievement of the overall project goal of providing reliable and economical analysis capabilities for geotechnical engineering structures.

The results of the research conducted prior to this contract and sponsored by various agencies including NCEL is summarized in reference [1]. Of the several phases of the overall project, the model validation phase is in many ways the most challenging and in some sense never ending. The problem is that the range of stress histories that can occur in a geotechnical structure during its service life, and thus the required range of a truly comprehensive constitutive model, is limitless. Thus, it is never really possible to completely verify a comprehensive three-dimensional constitutive model for a complicated material such as soil. Practically the verification must be limited to simple examples representing certain general classes of stress histories including drained and undrained conditions, three-dimensional states, non-proportionate loading, cyclic conditions, rotating principal stress directions, etc. Unfortunately a number of these conditions are difficult to achieve in simple laboratory tests. In addition, the presence of a high degree of material variability in a material such as soil greatly complicates the task. In the initial phases of the project experimental data published in the open literature for various cohesive soils were used both to suggest the phenomena that needed to be modeled and for validation studies to establish the correctness of the model. However, it soon became apparent

that a data base (for a single type of cohesive soil) sufficiently large to permit a really thorough verification of the bounding surface model (or any other proposed general model) does not exist. Thus, a program was initiated at Davis to generate, for a particular cohesive soil, a more general data base than was available. The work carried out under this contract and reported herein represents a portion of this effort; additional results will be contained in [12].

For any material model to be of value, a well defined systematic procedure must be available for calibrating the model in terms of simple test results. A trial-and-error, computer aided calibration procedure for the bounding surface model is reported in reference [1]. The calibration reported herein followed this procedure except for a minor modification which is described in a later section. The application of the method, however, requires considerable experience and judgement on the part of the analyst. Thus, a more fully automated computer aided scheme requiring much less subjected judgement is presently being developed under NSF and University sponsorship. This procedure will use a quasi-Newton method to select the model parameters so as to minimize the sum of the squared differences between experimental observations and model predictions for the calibrating experiments. The procedure will be carefully documented and illustrated in [13].

2. Experimental Program

Since the introduction of consolidation theory by Terzaghi, the concept of constitutive laws for the prediction of soil behavior has been well established in geotechnical engineering. The ever increasing use of electronic computers coupled with the development of highly efficient numerical analysis scheme requires more sophisticated soil models for the accurate prediction of soil behavior than available in the past. As a result many theories for describing constitutive relationships of soils have been proposed in recent years.

The merit of a constitutive relation, however, has to be evaluated and subsequently verified by a rigorous and carefully designed laboratory testing program of soil samples under various types of loading conditions and paths to failure. Unfortunately, many of the currently adopted constitutive relationships for soils have been established on a limited data base for special loading conditions. Consequently, there is a growing demand for more extensive and reliable laboratory test results that can be used to develop more accurate soil characterizations.

The experiments of the current study were conducted using laboratory prepared saturated clay specimens, and included triaxial compression and extension tests, thick-walled cylinder tests, and consolidation test for measuring the k_0 -stress ratio. The details of the testing program are presented in the following sections.

2.1 Mixing and Slurry Preparation

In order to obtain useful tests results it is important that, in addition to applying accountable stress histories, all soil specimens are of identical composition. Such specimens can only be formed by consolidating soil slurry in the laboratory. The soil used for this study is a kaolin soil chosen for its relatively high permeability, thus requiring shorter time for consolidation. The

commercial name of the kaolin, available from the Georgia Kaolin Company, is SNO-CAL 50.

To minimize the effect of consolidation related material anisotropy (the alignment of clay particles perpendicular to the direction of the major principal stress during 1-D consolidation), the slurry is only consolidated with a pressure sufficient to insure that handling of the consolidated material is possible; i.e. to obtain sufficient cohesion for holding the soil block together upon extrusion from the consolidation mold, and the subsequent trimming to form test specimens of required dimensions. It is found that the addition of 5% Bentonite (by weight) into the kaolin can, for the same consolidation pressure, greatly increase its strength without any drastic reduction in permeability. The grain size distribution of the kaolin mixture along with its other physical properties are given in Figure 2.1.

The slurry is obtained by mixing weighed portions of air-dried soils with de-aired, de-ionized water to give a mixture with approximately 3 times the liquid limit of the desired soil. The mixing is done with an electric mixer for about an hour. Air bubbles in the slurry, introduced as a result of mixing, are later removed by passing the slurry through a #120 standard sieve. The remaining entrapped air is further freed by transferring the sieved slurry to a specially designed vacuum-mixing vessel. This vessel is then placed on a small shaking table for several hours during which time a vacuum of 85 kPa is applied and the slurry is stirred intermittently. At the end of the mixing process, the slurry is carefully poured into a consolidated mold and placed in a loading frame for initial consolidation.

2.2 Initial 1-D Consolidation and Sample Preparation

Aluminum molds (6" I.D. and 16" long) are used for initial consolidation of the slurry. The inside walls are plated and a thin layer of high vacuum stopcock grease coat is applied to reduce the wall friction. To prevent leakage of slurry from the mold, a thin plexiglas, ring-shaped washer is placed between the bottom porous stone and the circular filter paper. A similar ring is also provided for the top porous stone. The lateral earth pressure developed during consolidation is measured by a 3/4" diameter pressure transducer installed with its sensing tip flush with the inside wall of the mold. A total of three pressure increments are applied to reach the desired initial consolidation pressure of 14 psi (98 kPa). The consolidated soil block is then extruded from the mold and cut vertically into three equal pieces. They are wrapped in saran sheets and stored in the moisture room for a period of a few hours to a few days. For isotropic consolidation and shear testing a cylindrical sample (2.5" dia and 5" long) is carefully trimmed from the cut piece and properly mounted in the triaxial cell. A specimen for a thick-walled cylinder test is obtained by placing an entire consolidated soil block in a special mold in which it is possible to trim out a 4" diameter core thus forming a one inch thick soil tube.

2.3 Testing Apparatus and Procedures

A constitutive relationship describing the fundamental behavior of soil is generally expressed by considering a point in a continuum; i.e. an infinitesimal element of a soil mass having a homogeneous state of stress and strain and free from boundary constraints. Therefore, an ideal test is one which satisfies exactly

the above conditions, i.e. one for which all points within the soil specimen experience the same stress and strain states. Regrettably, none of the available soil testing apparatus completely meet this requirement, primarily due to the friction between the loading platen and the soil, which restricts the lateral expansion or contraction of the sample at and near its ends. To minimize this problem every effort was made to reduce the boundary effect for the triaxial and the thick-walled cylinder testing apparatuses used in the present study.

2.3.1 Triaxial Testing Apparatus: One of the most commonly used soil testing device is the triaxial testing apparatus. Bishop and Henkel [2] presented an in-depth description of the device as well as the associated testing procedure. Modifications and discussions of the apparatus in the ensuing years by many researchers have made it a widely acceptable device capable of producing reliable test results. Conventionally, porous stones are placed between the top and bottom platens and the specimen serving as filters for the flow of water in and out of the specimen. A major disadvantage of this arrangement is the constraint on free expansion or contraction in the end zones of the specimen. Many attempts have been made [3,4] to develop a "frictionless" platen. Experimental evidence has shown that the most effective way of reducing end friction is to place a lubricated thin membrane directly between a polished platen and the ends of the specimen. In the present study, two circular membranes with slits and lubricated with silicon grease, are placed between the platens and the specimen. To maintain the flow of water, a $\frac{1}{8}$ " porous bronze disc is embedded in the center of each platen and connected to the drainage path.

Because of the relatively long period of time required for testing, Dow Corning 1102 silicon fluid is used to fill a perspex jacket placed around the sample inside the triaxial cell. The fluid serves as a buffer separating the soil from the water in the cell thus minimizing the possibility of air entering into the saturated soil specimen. In addition to this provision, the cell water, during the isotropic consolidation phase, is flushed regularly with de-aired water in order to reduce the amount of entrapped air.

During isotropic consolidation, the volume and height changes of the sample are measured with a graduated "U" tube (accurate to 2/100 of a c.c.) and a mechanical dial gage (accurate to 0.001 in) respectively. Changes in sample diameter are calculated assuming that uniform radial deformation of the specimen has occurred. The isotropic consolidation pressure (cell pressure) is applied in 5 increments up to a magnitude of approximately 4 times the initial consolidation pressure. It is generally accepted that when a consolidation pressure of 3 to 4 times the level of the previous maximum pressure (the k_0 -stress state) is applied, any anisotropy of the soil fabric will be nearly destroyed as a result of particle re-orientation under relatively large deformation. The different OCR samples are formed by reducing the effective confining pressure in one increment (isotropic rebound) to the desired value.

2.3.2 Thick-walled Cylinder Testing Apparatus: A major disadvantage of the triaxial apparatus is that the principal stresses cannot be controlled independently (i.e., $\sigma_2 = \sigma_3$ or $\sigma_2 = \sigma_1$). Other devices have been suggested for simulating "true triaxial" states of stress by controlling the three principal stresses independently. These devices often yield non-homogeneous stress distributions and/or limited strain measurements and often require cumbersome sample preparation. The most commonly proposed test of this type uses a cubic soil sample. A hollow cylindrical sample is an alternative to the cubical sample.

Originally hollow cylindrical samples were used in torsional tests to produce a non-homogeneous, pure shear stress state. Samples tested in this device are usually subjected to isotropic states of stress prior to torsion. By using loadings other than torsion, it is possible to perform tests which produce three independent principal stresses. For instance, by independently controlling the axial, inside and outside pressures, independently varying axial, tangential, and radial stresses in the soil may be obtained. The resulting non-homogeneity of the stress state is either approximated as homogeneous or analyzed numerically. Among all possible combinations of stress states that can be produced in this manner two sets are of particular interest for soils. First, the condition of plane strain can be simulated in hollow cylinder samples if the axial movement of the specimen is prevented and secondly by either increasing the inside pressure or decreasing the outside pressure tensile stresses (in the circumferential direction) can be induced in the soil.

The testing device fabricated for the present study is similar, with minor modifications, to the one described by Al-Hussaini and Townsend [5]. Fig. 2.2 shows the details of the apparatus. The ring shaped end platens, made of polished perspex, are used to seat the sample. Six porous bronze discs are embedded in each platen to provide the drainage passage for water. Using a special mold and tools, samples are trimmed to form a hollow cylinder 6" high with 4" I.D. and 6" O.D. Rubber membranes are used to cover both the inside and outside walls of the hollow specimen. The inside cavity is separated from the outer cell and is filled with water; water also fills the cell and surrounds the specimen. Volume changes during consolidation are measured by two graduated "U" tubes; one connects to the inside cavity and the other to the sample itself. The change of outside radius is recorded using 3 LVDT's spaced at 120° around the sample and placed at different heights. The total height change of the specimen is measured by a mechanical dial gage attached to the loading rod. Thus, assuming that the hollow cylinder remains axisymmetric its deformed geometry can be determined using the information obtained from the various sensing elements described.

2.3.3 Testing Machine: The testing machine used for this investigation is a specially designed three hydraulic actuator, microprocessor controlled, closed loop system built by Cox & Sons. The system is programmed so that the machine control functions are interrupt driven (background) routines allowing use of the foreground for data display, program input, program edit, report generation, equipment diagnostics, direct manual operation, etc. as selected by a mode selection switch.

A standard industrial grade printed circuit board is used as the Central Process Unit (CPU). It contains the microcomputer, memory, parallel digital Input and Output (I/O) and two serial data ports. The main serial port drives the system terminal at approximately 1000 characters per second (9600 BAUD). The second serial port is used for program and data output.

The memory expansion module contains additional Random Access Memory (RAM) and Programmable Read Only Memory (PROM). The PROM contains the system software (FORTH with monitor, editor, and assembler), the machine control software and the standard test control, data acquisition, data reduction and report writing modules. Additional test control, data reduction and report writing routines can be loaded using a punched tape reader.

The three axis analog controller controls the main (vertical) actuator in both load and stroke modes, the confining pressure in load control and a third axis (which can be used for internal pressure or torsion control, etc.) with both load and stroke feedback.

The front panel of the system is used to select the operation mode and for manual positioning. A Video Display Terminal (VDT) is used for data display during manual controlling or actual specimen testing. The VDT is also used for complete operator control, program editing, machine diagnostics, etc.

Data may be acquired by two methods. It may be buffered to memory during the test or may be printed out on the system printer. Memory buffering is useful for high speed data acquisition of limited amounts. The printer is more appropriate for long term testing where large amounts of data are to be collected. A third method for continuous data collection is to attach a recorder to the system.

This system is capable of recording deformation to .0001", load to 0.2 lbs, pore pressure to .1 psi, volume change to .1 cc, and cell pressure to .1 psi. The fully automated testing system ensures the high quality of experimental results necessary for material characterization.

3. Description of Experiments

An extensive set of undrained compression (intermediate principal stress equal to the minor principal stress) and extension (intermediate principal stress equal to the major principal stress) triaxial tests of different OCR values were performed for this investigation. The results of these tests were used in both the calibration and verification phase of the research project as described in the next section. A limited number of drained triaxial tests and several specially designed triaxial as well as thick-walled cylinder tests were performed to further check the predictive capabilities of the model (results beyond what are reported herein are to be found in [12]). Most of the tests were of the strain-controlled type; however, some of the specially designed tests were performed under load-controlled conditions. Table 3.1 lists relevant information for the various samples tested. As stated previously, all samples were first consolidated under an isotropic stress (i.e. $q=0$) of approximately 392 kPa. For overconsolidated samples the effective confinement was then reduced. Brief descriptions of these tests are given below.

3.1 Isotropic Consolidation

Samples were mounted in triaxial cells and subjected to further consolidation and swelling to a specified overconsolidation ratio. For each pressure increment (decrement), axial and volume change readings were taken to determine the dimensions of the sample. Typical volume and height changes vs time relationships measured during isotropic consolidation are depicted in Fig. 3.1. Fig. 3.2 gives the volume and height changes for swelling. At the end of each step the void ratio was calculated from its initial value and subsequent changes.

The relationship between the void ratio, e , and the effective mean normal pressure, p' , is customarily shown on a semilog scale where natural logarithm

values of p' are used. Fig. 3.3 depicts the range and mean value of the void ratio for each pressure increment. It can be seen that the e - $\ln p'$ relationship can be represented reasonably well by an equation $e = e_1 - \lambda \ln p'$ for mean values of e , where e_1 is the value of the void ratio for $p' = 1.0$ kPa, and $\lambda = 0.15$. Similarly the swelling behavior can be represented by $e' = e_0 - \kappa \ln(p'/p'_0)$ where e_0 and p'_0 refer to the point on the virgin compression curve prior to swelling and $\kappa = 0.018$ (λ and κ are two of the classical critical state soil parameters [6]).

3.2 Deviatoric Stress

Axial stress-strain relationships for samples tested in compression and extension are shown in Fig. 3.4. The influence of the mean normal effective stress and overconsolidation ratio on stress strain behavior are shown on a normalized scale in Fig. 3.5. It can be observed that the magnitude of the deviatoric stress increases rapidly up to strains of about 1% and levels off after strains of about 3% with a smooth transition in between.

Since all tests were strain controlled, the axial strain at which the maximum deviatoric stress was reached can be determined. The maximum stress occurred at about 6% axial strain after which the deviatoric stress dropped slightly.

3.3 Pore Water Pressure

When the volume change is restricted, application of stress on a soil element results in the development of pore water pressure. The study of pore pressure response is important from both a practical and a theoretical point of view since the effective stresses (total stress minus pore water pressure) are mainly responsible for soil behavior.

Pore water pressure is plotted against axial strain in Fig. 3.6. It can be seen from this figure that the pore pressure depends on, among other factors, stress history (OCR); its magnitude decreases as the overconsolidation ratio increases.

3.4 Stress Paths

The undrained stress paths for normally, lightly, and heavily overconsolidated samples, tested in compression and extension, are plotted in Fig. 3.7. It can be observed that compressive undrained paths for normally and lightly overconsolidated samples are initially almost vertical followed by rapid decreases in p' . Similar behavior is also observed for stress paths in extension.

An interesting part of the undrained path is the behavior of the sample near failure. The value of the shearing stress q drops for all samples and pronouncedly forms the critical state line, CSL, which can be expressed as $q = M p'_f$, where M is the slope of the line (M is one of the classical critical state parameters [6]). This marked feature is as obvious for negative q . In general, the test results for samples in extension are less reliable than for compression. This results from the fact that during the course of an extension test the sum of the upward forces acting on the top platen becomes equal to the sum of the downward forces and thus, the top platen may separate from the sample. This phenomenon was observed particularly for heavily overconsolidated samples; once the separation occurred there was a drastic

necking at one end of the specimen. The values for M were 1.25 and .95 for compression and extension respectively. Similar differences were reported by Parry and Nadarajah [7] and Banerjee and Stipho [8].

4. Comparison of Model Predictions and Experimental Results

4.1 Method

As has been previously stated, the primary purpose of the laboratory testing program outlined in chapters 2 and 3 was to enable the predictive capabilities of the bounding surface model to be more fully examined. Hence, in the sections which follow, comparisons will be made between the model predictions and the experimental observations.

However, before any predictions can be attempted, the constitutive parameters which define the shape of the bounding surface and the subsequent soil response must first be identified. Since a complete discussion of the various model parameters has been presented in [1], no additional description will be provided here.

Most of the model parameters, including the traditional critical state properties, may be obtained directly by simple laboratory testing. However, the remaining constants must be indirectly established through a trial-and-error curve fitting or "calibration" procedure. The specific features of this manual calibration process have been described in detail in reference [1], together with a documented example and various calibration guides. An automated calibration code is currently being developed, and will be reported in [13].

In the present study the bounding surface model will be calibrated by means of the manual procedure described in reference [1]. The results from the undrained triaxial compression tests run at overconsolidation ratios of 1, 2 and 6, and the extension tests run at overconsolidation ratios of 1, 2 and 12 will serve as the basis for the model calibration. Then, with the required constitutive parameters having been established, the model will next be used to predict the results of the remaining laboratory experiments described in chapters 2 and 3; namely, the:

- i) undrained triaxial compression tests at OCR=1.3, 4 and 12;
- ii) undrained triaxial extension tests at OCR=1.3 and 4;
- iii) drained hollow-cylinder series; and,
- iv) drained triaxial series.

4.2 Model Calibration

The calibration was initially performed using the model as described in reference [1], in which the projection point is fixed at the origin. Some of the trial calibration curves are shown in Figures 4.1, 4.2 and 4.3, in which the experimental observations and model predictions are compared for undrained triaxial compression tests run at overconsolidation ratios of 1, 2 and 6.

As may be seen in Figure 4.1, the model (with fixed project point) fails to capture the observed q vs. p' response (and, to a lesser extent, in Figure 4.3, the experimental u vs. ϵ_1 response) exhibited by the soil at overconsolidation

ratios of 2 and 6. At these overconsolidation ratios the laboratory specimens shown an initial increase in p' upon shearing, whereas the predicted response showed an initial decrease.

A review of available experimental literature has revealed that certain overconsolidated soils show an initial increase in p' upon shearing, while others show an initial decrease. For example, the experimental works of Balaonbramaniam and Chaudhry [9] and Banerjee and Stipho [8,10] indicate that an overconsolidated clay will exhibit an initial decrease in p' upon shearing. The laboratory observations cited by Parry and Nadarajah [7] on the other hand, suggest just the opposite. This difference in behavior may possibly be due to a fundamental difference in the soil properties. However, since the clay used in the present study (see chapter 2) is very similar to that used by Banerjee and Stipho [8,10], the observed difference in soil behavior may actually be an artifact of the laboratory procedure or testing apparatus of one or more of the laboratories. With this possibility in mind a thorough analysis of our own procedures was made; this investigation did not reveal any problems.

In either event the results of the initial calibration attempt demonstrated the need to generalize the model slightly in order to be able to model either type of behavior. Hence, a new parameter "c" has been introduced which permits a point other than the origin to be selected as the projection point for the bounding surface (see reference [1] for a comprehensive discussion of the projection rule).

Several important questions concerning the modified mapping rule remain to be answered. The full practical and theoretical implications and potential of using a mapping point other than the origin remain to be explored; this task is one component of a proposed future study. The apparent contradictory experimental evidence alluded to above, will need to be reconciled in the proposed study and the actual importance of the phenomena in question will need to be established by means of a sensitivity study.

Due to the introduction of this additional model parameter, it was necessary to slightly modify the manual calibration procedure outline in reference [1]. It may be noted that the location of the projection point, and thus the value of the parameter c, has no effect on the response of a normally consolidated soil. It was also found that the parameter c has little or no influence on the predicted q vs. ϵ_v response. Hence, the optimal value of c may be selected by examining the q vs. p' response of the overconsolidated samples included in the calibration basis.

In order to more clearly illustrate the influence of c on a soil's q vs. p' response, and thereby facilitate the suggested manual calibration procedure, the relative influences of the hardening parameter h_c and the projection point parameter c have been compared in Figures 4.4 and 4.5. These figures show the q vs. p' behavior of a soil at an overconsolidation ratio of 2 subjected to undrained triaxial compression as predicted by the model for a range of values of h_c and c.

As may be seen in Figure 4.4, the hardening parameter h_c has a large influence on the shape of the q vs. p' curve for large values of q , but only a rather small effect for small values of q . The projection point parameter c, on the other hand, has a very large influence on the slope of the q vs. p'

response when the soil is initially sheared. In other words, of the two parameters, c has the larger effect on the angle which the q vs. p' curve makes with the p' -axis.

Hence, it is suggested that the optimal value of c be selected by fitting the model predictions to the initial portions of the experimental q vs. p' curves. Then, the parameters h and A may be established through the procedure outlined in reference [1]. It should be noted that the parameter c must assume the same value in both compression and extension. Thus, in choosing a value of c , both sets of experimental observations should be considered.

By means of the approach outline above, calibration of the model using both triaxial compression (Figures 4.6, 4.7 and 4.8) and triaxial extension (Figures 4.9, 4.10 and 4.11) data was readily obtained. A comparison of Figures 4.6, 4.8, 4.9 and 4.11 to Fig. 4.1-4.3 shows quite clearly that the new parameter c permits the model predictions to much more closely approximate the observed experimental soil response.

The agreement between the predicted and measured q vs. p' curves shown in Figure 4.6 for compression and Figure 4.9 for extension is quite good, particularly for $OCR=1$ and 2 in compression and $OCR=1$ and 12 in extension. The similarity between the predicted and observed q vs. ϵ_1 responses shown in Figures 4.7 and 4.10 is also quite good. The failure of the model to predict the "falling" portion of the q vs. ϵ_1 curves observed in both compression and extension at high values of axial strain ϵ_1 is most likely due to the loss of homogeneity in the samples for large strains and/or because large deformation effects have not been included in the model predictions (the modifications required in the model to account for large deformations, will be made shortly in preparation for an international competition on modeling of soil behavior). Finally, the agreement between the predicted and measured u vs. ϵ_1 curves shown in Figures 4.8 and 4.11 is again remarkably close.

A complete list of the values of the model parameters established during the calibration process is presented in Table 4.1. For completeness, parameters corresponding to the old project rule (the projection point being fixed at the origin, $c=0.0$) and the generalized rule (with the projection point parameter c) are included.

4.3 Validation Study

Before comparisons are made between the model predictions and the remaining experimental observations one additional point deserves discussion. In comparing model predictions and experimental observations, the existence of material variability must be kept in mind. While variability is present for all materials, it is particularly important for a material such as soil. It is entirely an exercise in futility to demand greater accuracy of the constitutive model than the degree of variability present in the material. Nearly all the tests reported herein were repeated two or three times and the most typical results were reported. Figure 4.12 indicates the degree of variability observed for one of the test series. While sufficient data does not yet exist to permit a rational analysis of the importance of soil variability in the validation process it is hoped that it will be available in time for inclusion in [12] or [13]. At the present it suffices to note that such variability exists and for the most part it appears

that the model predictions fall within the scatter band of the experimental measurements (a rigorous discussion of a related topic can be found in [11]).

For a validation study to be of any value the model must be calibrated with one data base and then used to predict the results of a second independent set of experiments. Thus, the calibration process described above was made without any reference to the experimental results presented in the following sections.

4.3.1 Undrained Triaxial Compression Tests: Comparisons of the predicted and observed q vs p' , q vs. ϵ_v and u vs. ϵ_v responses for triaxial compression tests run at overconsolidation ratios of 1.3, 4 and 12 are shown in Figures 4.13, 4.14 and 4.15. The agreement between the model predictions and the experimental observations is rather close, overall. There is some discrepancy between the predicted and observed q vs. p' response (Figure 4.13) for OCR=4 and the q vs. ϵ_v response (Figure 4.14) for OCR=12. Significant deviations also exist between the predicted and observed u vs. ϵ_v responses for OCR=4 and 12. However, it is likely that at least some of these deviations are attributable to inaccuracies in the experimental pore-water pressure measurements for small absolute values of u .

4.3.2 Undrained Triaxial Extension Tests: Comparisons of the predicted and observed q vs. p' , q vs. ϵ_v and u vs. ϵ_v responses for triaxial extension tests run at overconsolidation ratios of 1.3 and 4 are shown in Figures 4.16, 4.17 and 4.18. Again, the agreement between the two sets of curves is quite good, overall. The similarity between the predicted and observed q vs. p' and q vs. ϵ_v responses is particularly close. Unfortunately, the u vs. ϵ_v curves show a much greater deviation. However, it is very likely that the discrepancies between the curves in Figure 4.18 may, to a large part, be due to inaccuracies in the experimental pore-water pressure measurements.

4.3.3 Hollow-Cylinder Tests: The results of the two thick-walled cylinder tests reported herein must be regarded as preliminary, further results will be given in [12].

Test #1: It was intended that the test be under drained, plane strain conditions, however, due to a procedural error and the rapidity of the test (≈ 5 hours) neither of these conditions were fully achieved. While the deviation from plane strain conditions could be approximately accounted for in the interpretation of the results, the deviation from drained conditions could not. The degree to which this problem contributed to the differences between the measured and predicted results is unknown. Visual observation indicated that a slight curvature of the initially straight vertical walls of the sample developed during the course of the test, however, it did not appear to be significant. The sample appeared to retain its axisymmetric geometry up to the point of failure, at which time a vertical shear plane cut the wall of the cylinder at one circumferential location. The inclination of the normal to the shear plane from a tangent to the circumference of the cylinder was about 30° . The initial OCR of the soil was 1.5; the preconsolidation pressure was 392.2 kpa and the all-around pressure at the beginning of the test was 260.6 kpa.

The test was intended to be plane strain with a constant internal pressure ($\sigma_i = 260.6$ kpa) and an increasing outer pressure ($\sigma_o = 260.6$ kpa \rightarrow) until failure

occurred. However during the first part of the test ($\sigma_z = 260.6 \rightarrow 286.8$ kpa) an undetermined amount of downward movement of the top platen inadvertently occurred resulting in non-plane strain conditions. It was possible to determine the history of the axial stress imposed on the sample during this portion of the test and thus it can be considered as specified ($\sigma_z = 260.6 \rightarrow 315.5$). At the point in the test when the error was discovered; the axial strain was very quickly brought back to zero, hence, momentarily producing undrained conditions followed by an unknown period of transient drainage. The test was then completed ($\sigma_o = 286.8 \rightarrow$ failure) as a plane strain test.

Even though end effects may be negligible the stress and strain states in the specimen are still inhomogeneous (functions of the radial coordinate). Two approaches for analyzing the test are considered. The first involves assuming that the cylinder wall is sufficiently thin that variations in the stress and strain can be ignored and the second is to perform a finite element analysis of the actual inhomogeneous fields.

Consider the first approach. If the cylinder wall is thin the following approximations can be made for the average radial and hoop stresses and strains (r_i and r_o are respectively the initial inner and outer radii of the cylinder and $u_i = \Delta r_i$, $u_o = \Delta r_o$ their respective changes).

$$\epsilon_r \approx - \frac{u_o - u_i}{r_o - r_i}$$

$$\epsilon_\theta \approx - \frac{u_o + u_i}{r_o + r_i}$$

$$\sigma_r \approx \eta \frac{\sigma_o + \sigma_i}{2}$$

$$\sigma_\theta \approx \eta \frac{r_o \sigma_o - r_i \sigma_i}{r_o - r_i}$$

Substituting the measured values for u_o and u_i (indirectly determined from change of the cavity volume) and the applied values of σ_o and σ_i , approximate histories of ϵ_r , ϵ_θ , σ_r and σ_θ are obtained. In addition the value of σ_z was specified for the first part of the test and measured for the second, and the value of ϵ_z was specified in the second part. Using σ_r , σ_θ and σ_z as input quantities for the first part of the test and σ_r , σ_θ and ϵ_z for the second part and approximating the stress and strain states as homogeneous the constitutive model was used to predict ϵ_r , ϵ_θ and σ_z (for the second part of the test). Comparisons of measured and predicted values are given in Figures 4.19 and 4.20. Predictions for u_i and u_o can be calculated from ϵ_r and ϵ_θ , these results are given in Figure 4.21. The point where the axial strain was suddenly brought back to zero is clearly evident in Figure 4.20.

In order to account for the inhomogeneity of stress and strain through the wall thickness a one-dimensional finite element analysis of the sample was

performed. A grid of four elements was found to be sufficiently fine. The predictions for u_i , u_o and the average value of σ_z are compared in Figures 4.20 and 4.21 to the measured values.

The causes of the discrepancies between the measured and predicted results certainly include the overall uncertainty concerning the degree of drainage due to the rapidity of the test, the inadvertent sudden change in axial strain (totally undrained) and possibly unaccounted for longitudinal variations in deformation. Even with these problems the comparisons may be viewed as satisfactory, although far from conclusive. The study clearly demonstrated (see Figures 4.20 and 4.21) the importance of accounting for inhomogeneities of stress and strain through the thickness of the cylinder.

Test #2: The second test was intended to achieve the plane strain, drained conditions that had been the goal of the first test. In order to achieve totally drained conditions the test was scheduled to be several days in duration. Two major problems developed. A previously unknown stability problem in the testing machine resulted in perturbations of the axial strain of unknown amounts and a laboratory accident (after five days of testing) destroyed the sample prior to completion of the test. Finite element predictions for the inner and outer surface displacements are compared, in Figure 4.22, to measured results for the portion of the test completed. Because of the control problem, these comparisons must be regarded as qualitative. Further thick-walled cylinder results will be reported in [12].

4.3.4 Drained Triaxial Tests: Because the effective and total stresses in drained tests are identical, such tests are particularly useful for achieving desired effective stress paths. The drained tests performed in this study were designed to investigate the consequences of arriving at the same final stress point via different stress paths. In the initial phase of this part of the study, a machine malfunction spoiled one test and made it necessary to run the series with alternate manually controlled equipment. Due to this problem and the excessive test time required (>20 days) to achieve drained conditions only three drained triaxial tests were completed; additional results will be reported in [12].

Tests #1 and 3: The first and third specimens were normally consolidated. A vertical path in p - q (see Figure 4.23) stress space was achieved by simultaneously decreasing the confining pressure while increasing the axial stress so as to maintain a constant mean pressure.

Test #2: The second specimen was preconsolidated to the same pressure as the first and third, and then allowed to swell to achieve an OCR of 2.1. From that point a three step path in p - q space was taken to reach the final series of states achieved in tests #1 and 3, see Figure 4.23.

Comparisons of predicted and measured results for tests #1 and 2 (test #3 duplicated #1) are given in Figure 4.24. The comparisons for volume change are excellent and those for the deviatoric stress q are satisfactory.

5. Summary and Conclusions

The experimentally observed soil response has served to justify the introduction of the new projection point parameter c which enables the projection

point for the bounding surface to be fixed at some location other than the origin. As a result of this additional model parameter, the manual calibration procedure outlined in reference [1] has been changed slightly. However, with the information provided in Section 4.2 and Figures 4.4 and 4.5, the determination of the parameter c becomes a relatively straightforward procedure.

The calibration and prediction curves given in Figures 4.6 through 4.24 enable the predictive capabilities of the bounding surface model to be more fully tested. The usefulness of the model as an analytical tool is verified by its ability to accurately capture experimentally observed soil responses in both triaxial compression and extension for a wide range of overconsolidation ratios. Indeed, the correlations shown in Figures 4.6 through 4.17 are even closer than those obtained using the experimental results of either Balasubramaniam and Chaudhry [9] or Banerjee and Stipho [8,10], which have been cited in a previous report [1]. The comparisons for drained triaxial conditions were also quite satisfactory, however, additional tests are needed for conclusive verification.

The use of the thick-walled cylinder test to achieve true three-dimensional states and its interpretation via the finite element procedure showed great promise, however, additional refinement of the test procedure is needed.

References

1. Herrmann, L.R., Dafalias, Y.F. and DeNatale, J.S., "Bounding Surface Plasticity for Soil Mechanics," Final Report to: Civil Engineering Laboratory, Naval Construction Battalion Center, Port Hueneme, Order No. USN N62583-30 M R478, Dept. of Civil Engineering, University of California, Davis, Oct. 1980.
2. Bishop, A.W. and Henkel, D.J., "The Measurement of Soil Properties in the Triaxial Test," Edward Arnold Pub., 1962.
3. Duncan, J.M., Seed, H.B., and Dunlop, P., "The Significance of Cap and Base Restraint in Strength Tests on Soils," Report No. TE-66-5, Dept. of Civil Engineering, Institute of Transportation and Traffic Engineering, UC Berkeley, Aug. 1966.
4. Rowe, P.W. and Barden, L., "The Importance of Free Ends in Triaxial Testing," Journal of the Soil Mechanics and Foundation Div., ASCE, Vol. 90, No. SMI, pp. 1-27.
5. Al-Hussaini, M.M. and Townsend, F.C., "Investigation of Tensile Testing of Compacted Soils," Miscellaneous paper S-74-10, U.S. Army Engineer Waterway Experiment Station, Vicksburg, Miss., 1974.
6. Schofield, A.M. and Wroth, C.P., Critical State Soil Mechanics, McGraw-Hill, London, 1968.
7. Parry, R.H. and Nadarajah, N., "Observation on Laboratory Prepared Lightly Overconsolidated Specimens of Kaolin," Geotechnique, Vol. 24, No. 3, pp. 345-358, 1974.

8. Banerjee, P.K. and Stipho, A.S., "Associated and Non-associated Constitutive Relations for Undrained Behavior of Isotropic Soft Clays," *Int. J. Numerical and Analytical Methods in Geomechanics*, 2, pp. 35-56, 1978.
9. Balasubramaniam, A.S. and Chaudhry, A.R., "Deformation and Strength Characteristics of Soft Bangkok Clay," *Journal ASCE Geotechnical Engineering Division*, Vol. 104, No. GT9, pp. 1153-1167, 1978.
10. Banerjee, P.K. and Stipho, A.S., "An Elastoplastic Model for Undrained Behavior of Heavily Overconsolidated Clays," *Int. J. Numerical and Analytical Methods in Geomechanics (Short Communication)*, 3, pp. 97-103, 1979.
11. Herrmann, L.R., "Effect of Edge Conditions on Test Results for Concrete," *International Journal of Cement and Concrete Research*, Pergamon Press, Inc., Vol. 8, pp. 25-36, 1978.
12. Jafroudi, S., "Experimental Verification of a Bounding Surface Plasticity Theory for Cohesive Soil," Ph.D. Thesis, University of California, Davis Campus, to appear Spring 1982.
13. DeNatale, J.S., "Calibration of a Bounding Surface Plasticity Model for Cohesive Soil," Ph.D. thesis, Dept. of Civil Engineering, University of California, Davis, to appear Summer 1982.

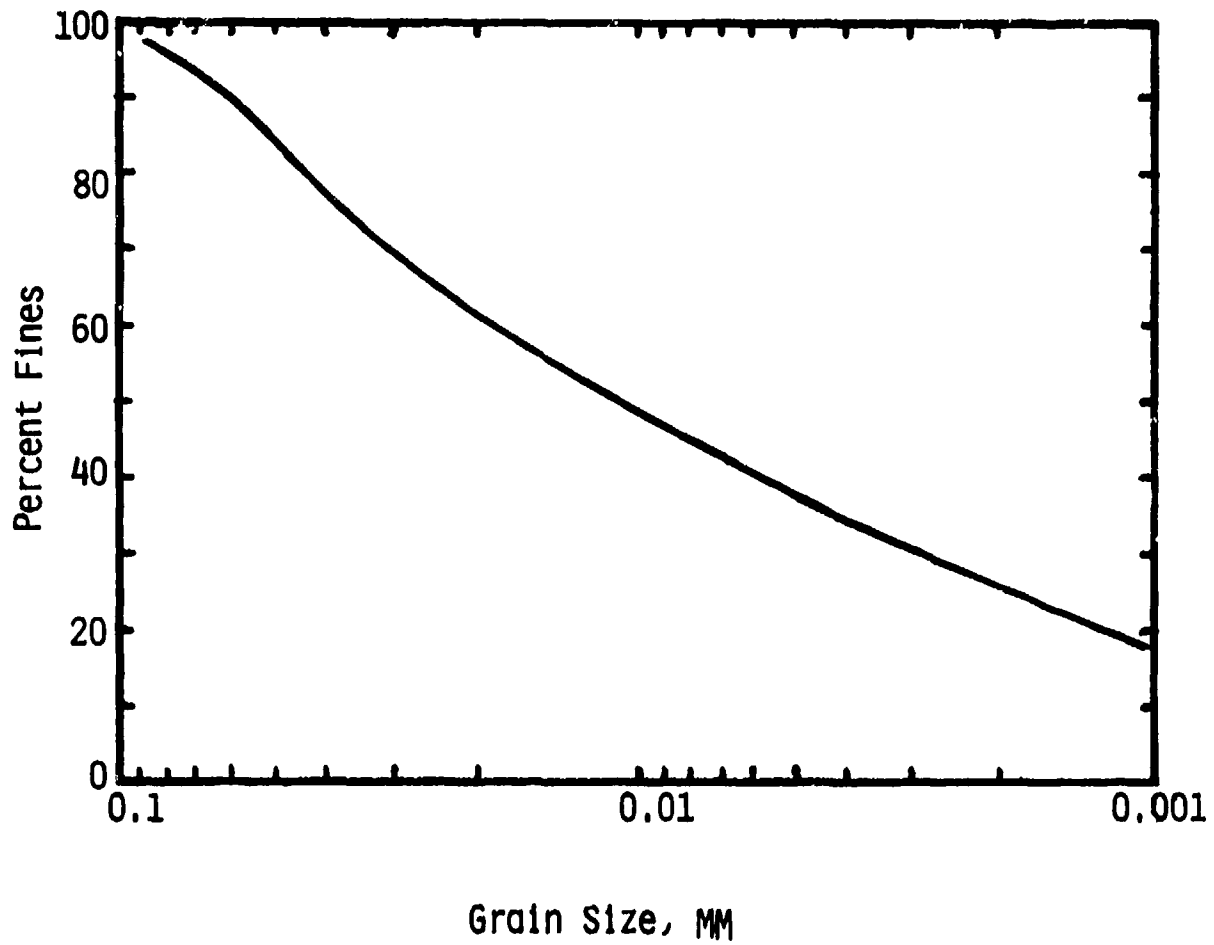
Table 3.1: Summary of Test Conditions

Sample I.D.	Max. Conf. Press, kPa	Conf. Press prior to test	OCR	Type of test
C1.0-1	392.2	392.2	1	CU
C1.0-2	392.2	392.2	1	CU
C1.3-1	392.2	304.0	1.3	CU
C2.0-1	392.2	196.1	2.0	CU
C2.0-2	392.2	196.1	2.0	CU
C4.0-1	392.2	98.1	4.0	CU
C4.0-2	392.2	98.1	4.0	CU
C6.0-1	392.2	65.3	6.0	CU
C6.0-2	392.2	65.3	6.0	CU
C12.0-1	392.2	32.7	12.0	CU
C12.0-2	392.2	32.7	12.0	CU
E1.0-1	392.2	392.2	1	EU
E1.0-2	392.2	392.2	1	EU
E1.3-1	392.2	304.0	1.3	EU
E2.0-1	392.2	196.1	2	EU
E4.0-1	392.2	98.1	4	EU
E12.0-1	392.2	32.7	12	EU
P1.0-1	392.2	392.2	1	Drained Constant P
P1.0-2	392.2	392.2	1	same as above
M2.5-1	392.2	156.9	2.5	Drained variable p-q
H1.5-1	392.2	261.5	1.5	Drained Hollow Cylinder
H1.5-2	392.2	261.5	1.5	same as above

Table 4.1: Model Parameters as Established Through The Manual Calibration Procedure

<u>Parameter</u>	<u>Projection Point at Origin</u>	<u>Projection Point not at Origin</u>
λ	0.151	0.151
κ	0.018	0.018
M_c	1.25	1.25
R_c	2.50	2.50
A_c	0.02	0.01
T^*	0.10*	0.10*
P_l^*	4.90*	4.90*
P_{o_i}	392.2	392.2
m_c^*	0.20*	0.20*
h_c	200.	300.
e_o	variable	variable
v	0.30	0.30
Γ	10^6	10^6
P_a	101.4	101.4
$n=M_e/M_c$	---	0.76
$\mu=h_e/h_c$	---	1.00
S	1.00	1.00
$r=R_e/R_c$	---	0.94
$a=A_e/A_c$	---	6.00
$V=M_e/M_c$	---	1.00
c	0.00	0.71

* As part of the present study an investigation was carried out which established and further demonstrated that even rather large charges in the assumed values of T , P_l , M_c and M_e have little or no effect on the predicted soil response.



L.L=47%

P.L=20%

$G_s=2.64$

Figure 2.1: Physical Properties of the Sno-Cal 50 + 5% Bentonite Soil

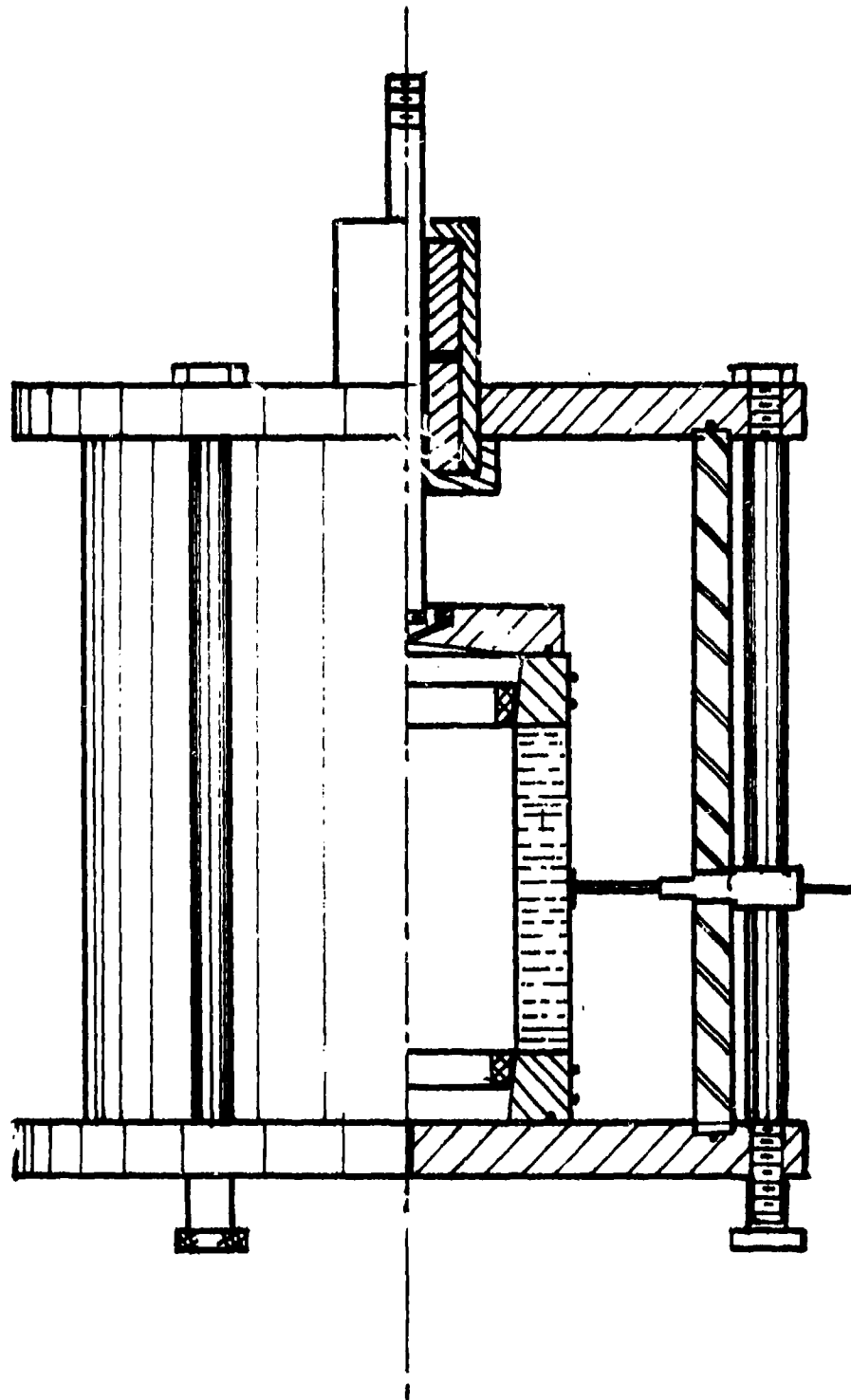


Figure 2.2: Hollow Cylinder Testing Apparatus

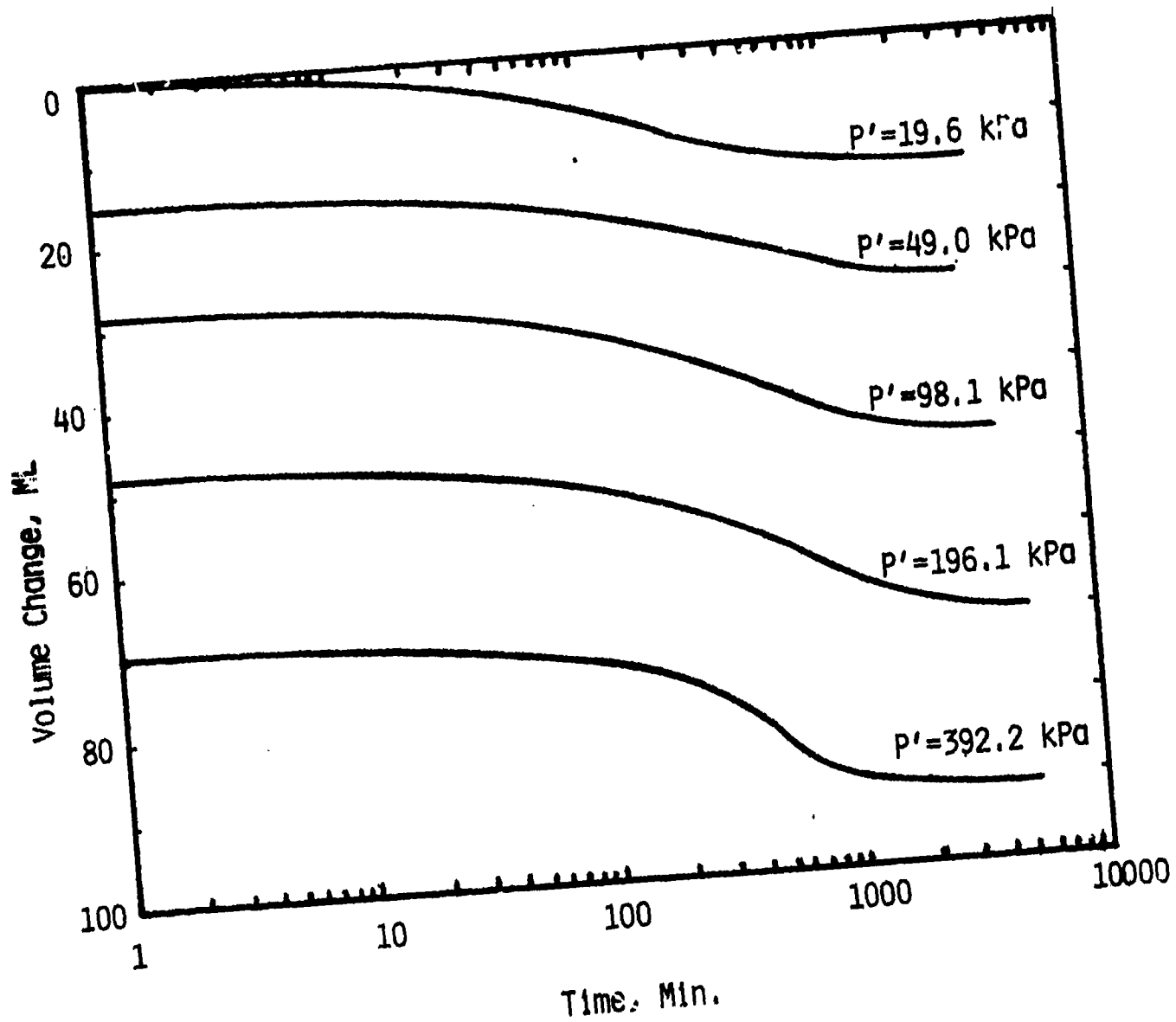


Figure 3.1a: Typical Volume Change During Isotropic Consolidation

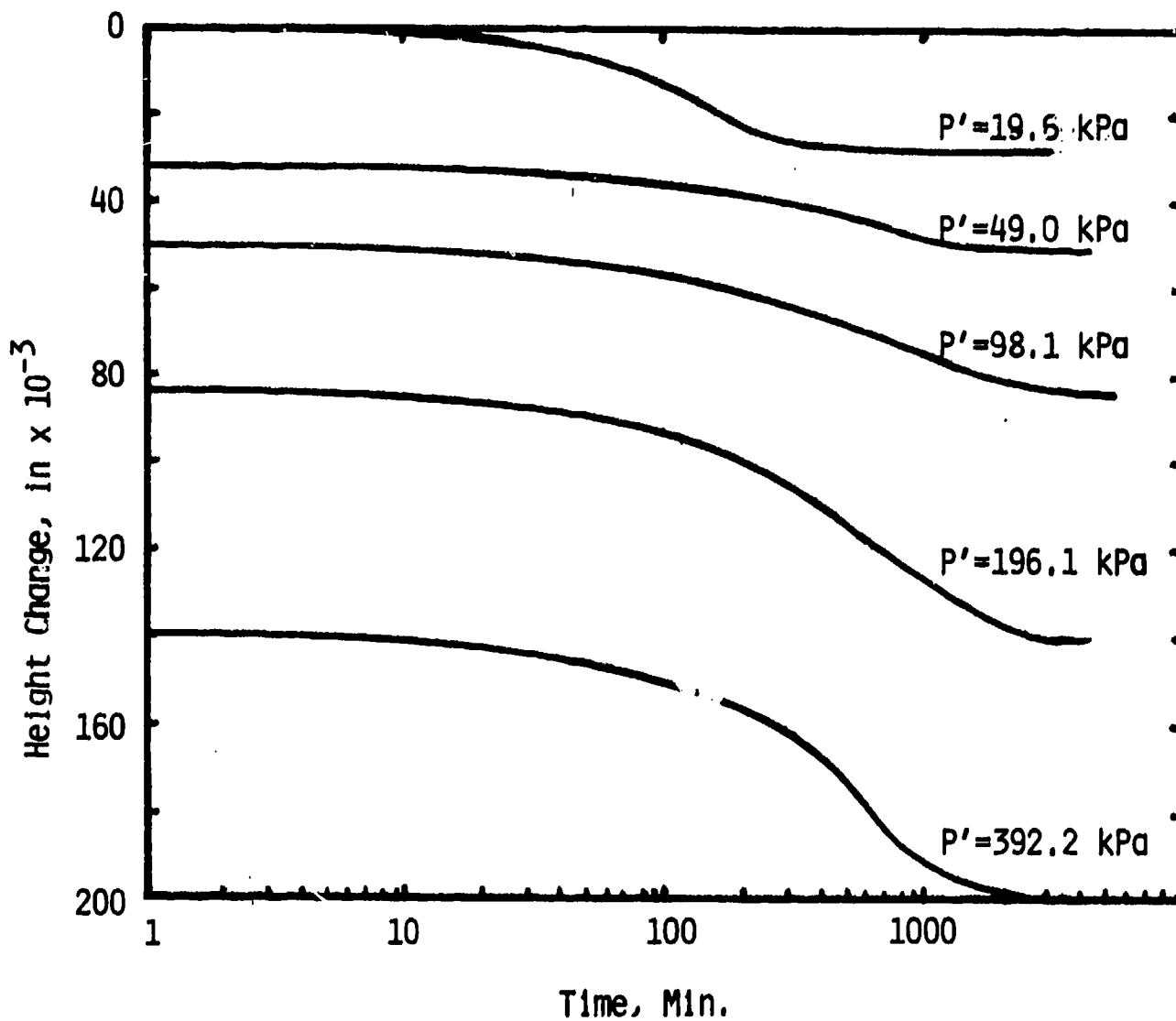


Figure 3.1b: Typical Height Change During Isotropic Consolidation

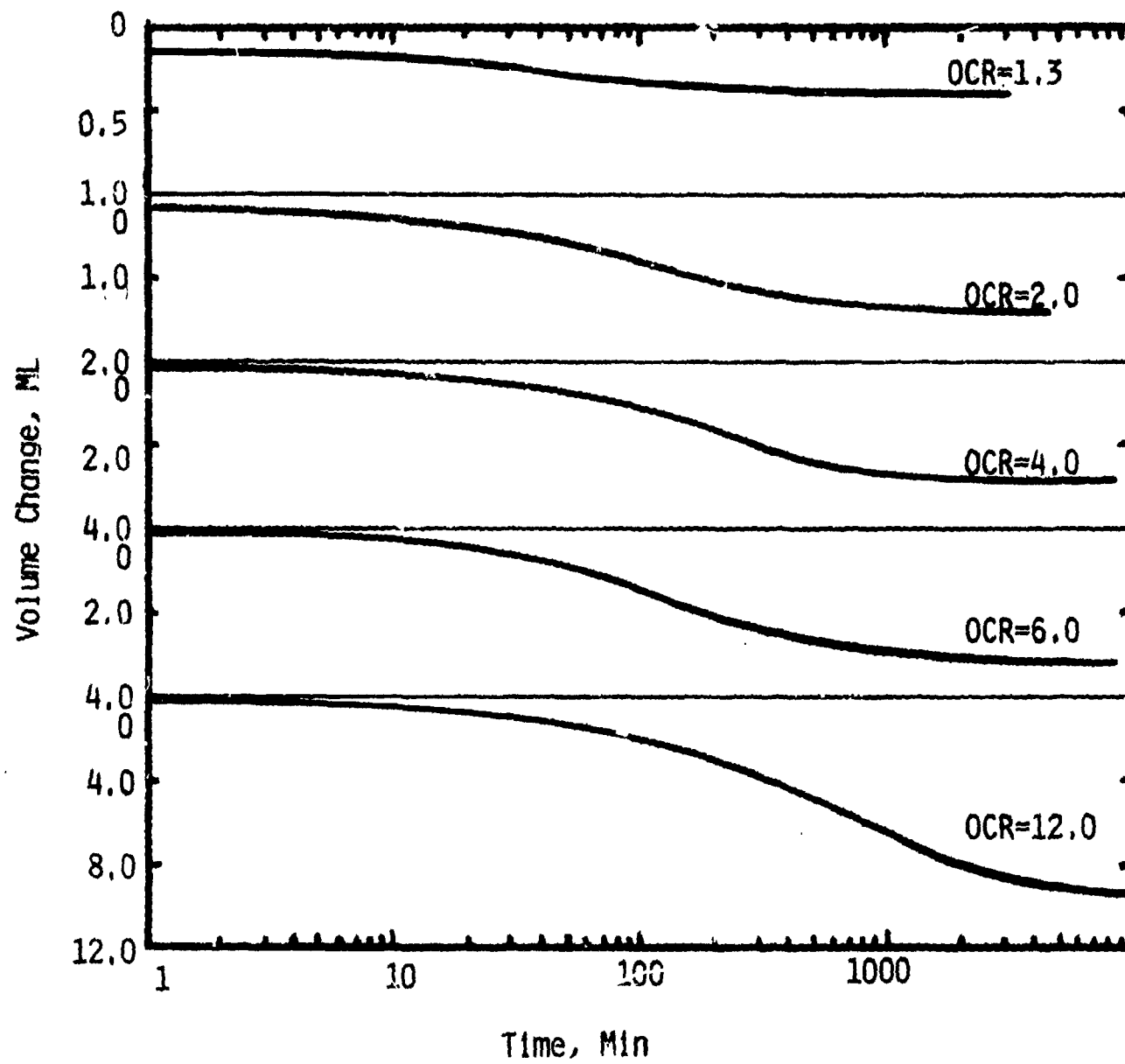


Figure 3.2: Typical Volume Change During Isotropic Swelling

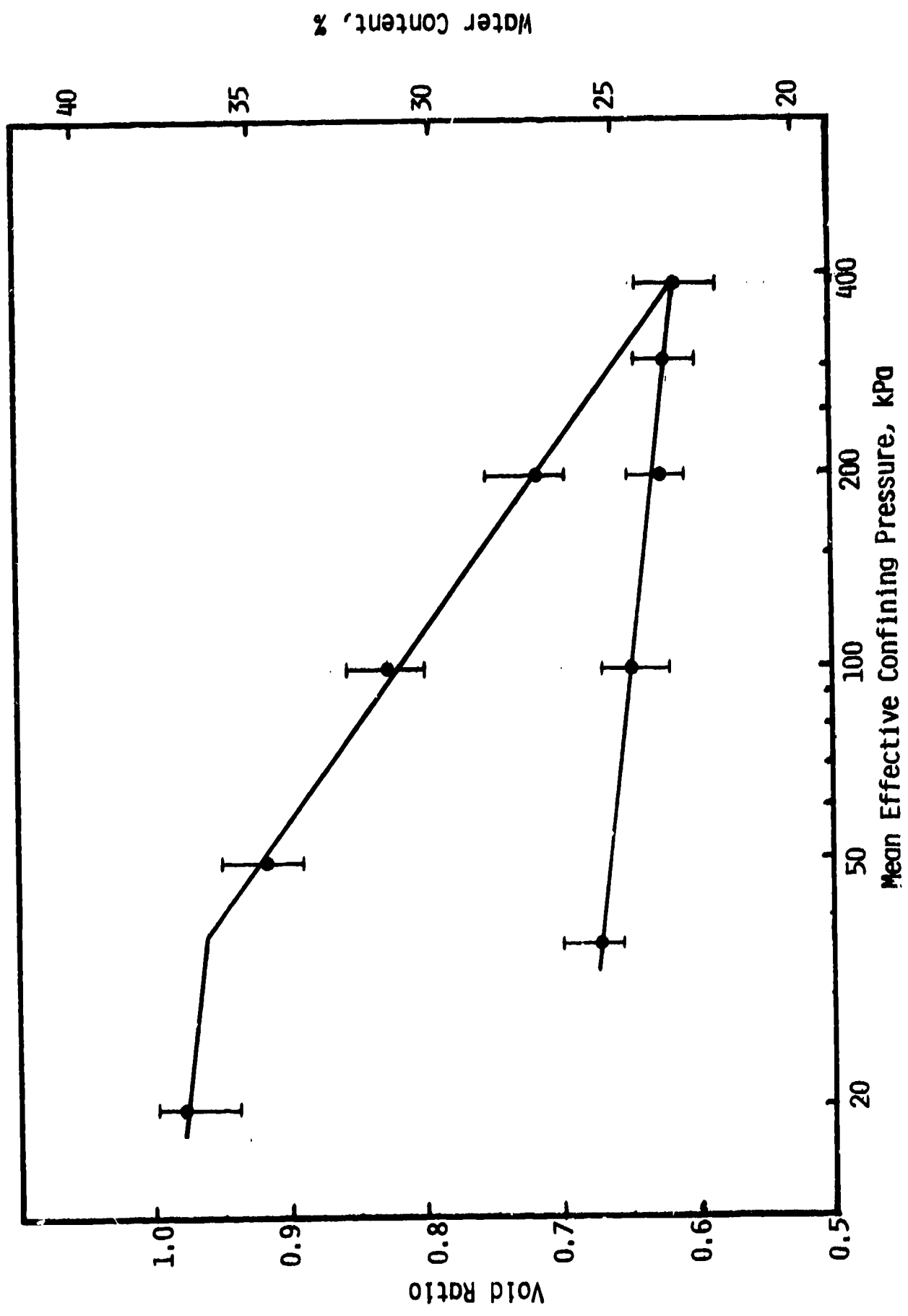


Figure 3.3: Relationship Between Void Ratio and Confining Pressure During Isotropic Consolidation

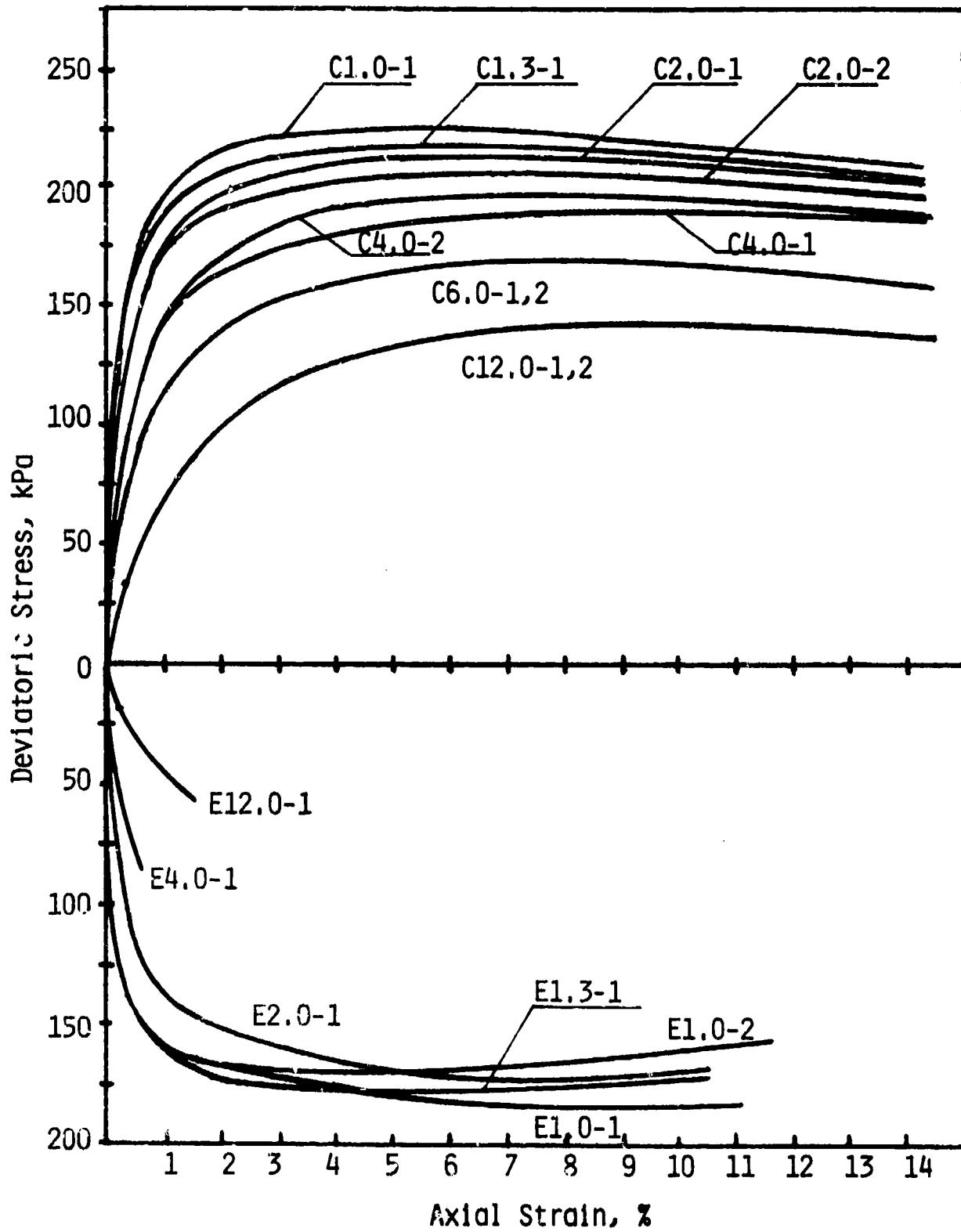


Figure 3.4: Axial Stress - Strain Relationships

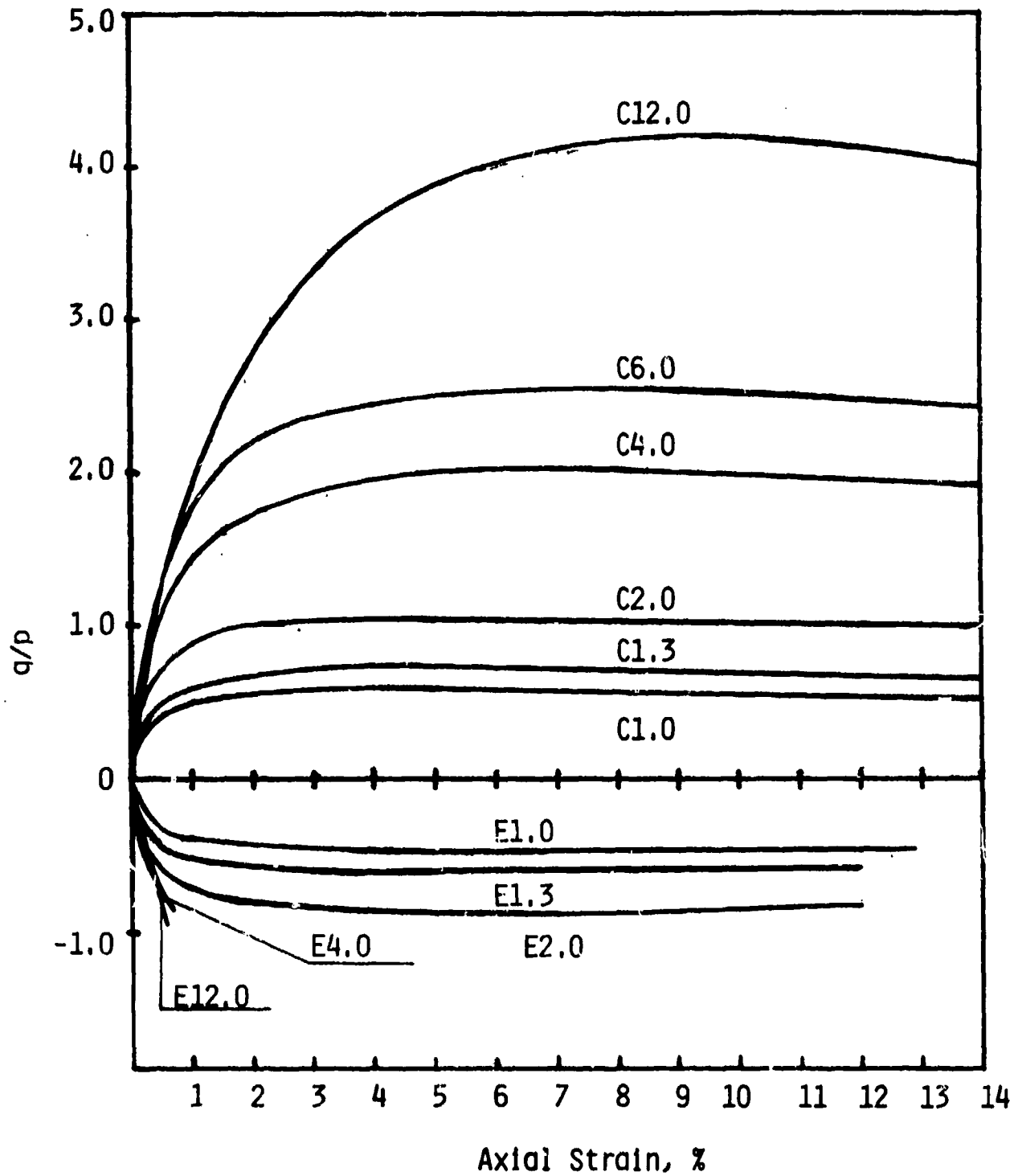


Figure 3.5: Normalized Axial Stress - Strain Relationships

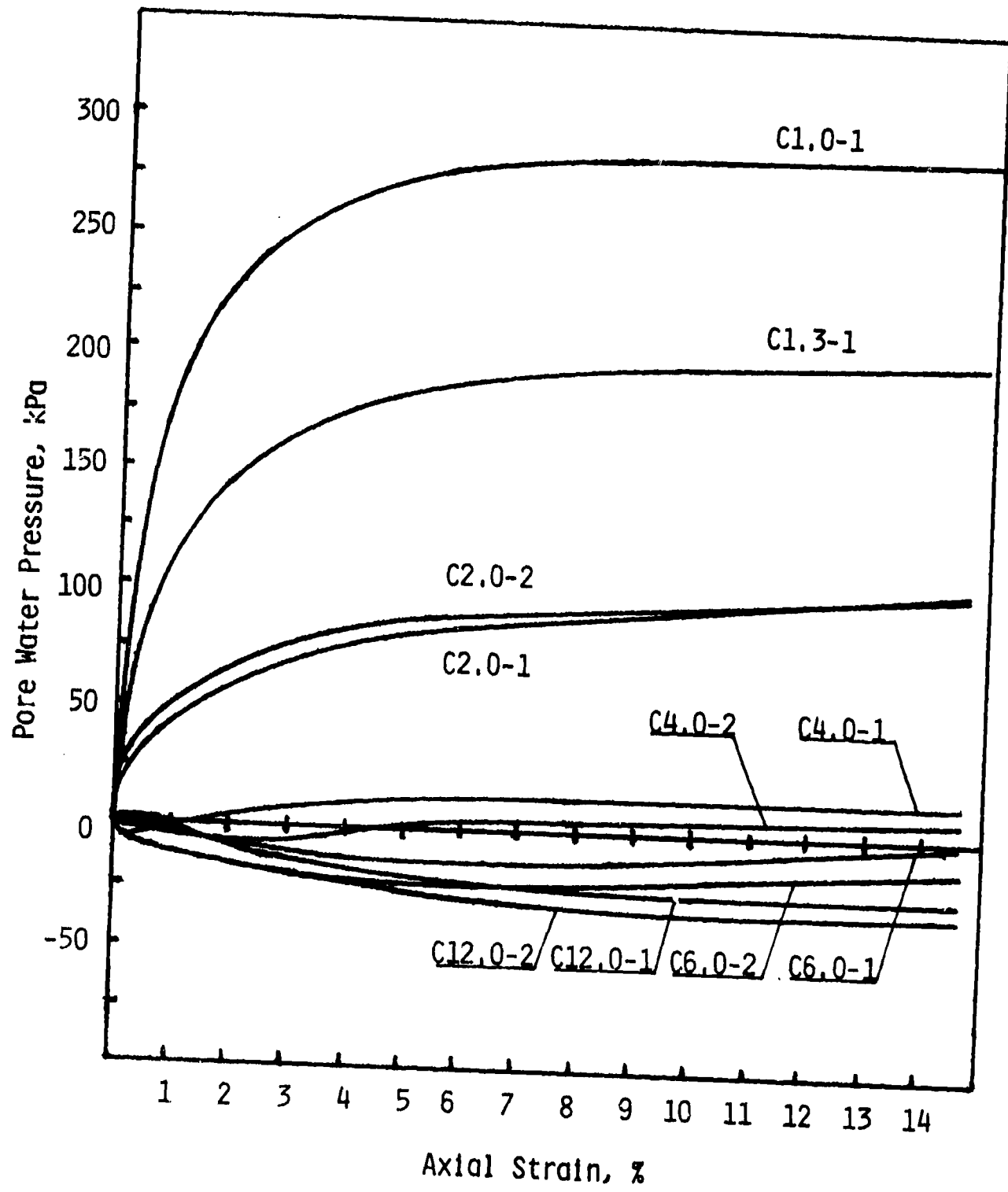


Figure 3.6a: Pore Water Pressure - Axial Strain Relationships For Compression Tests

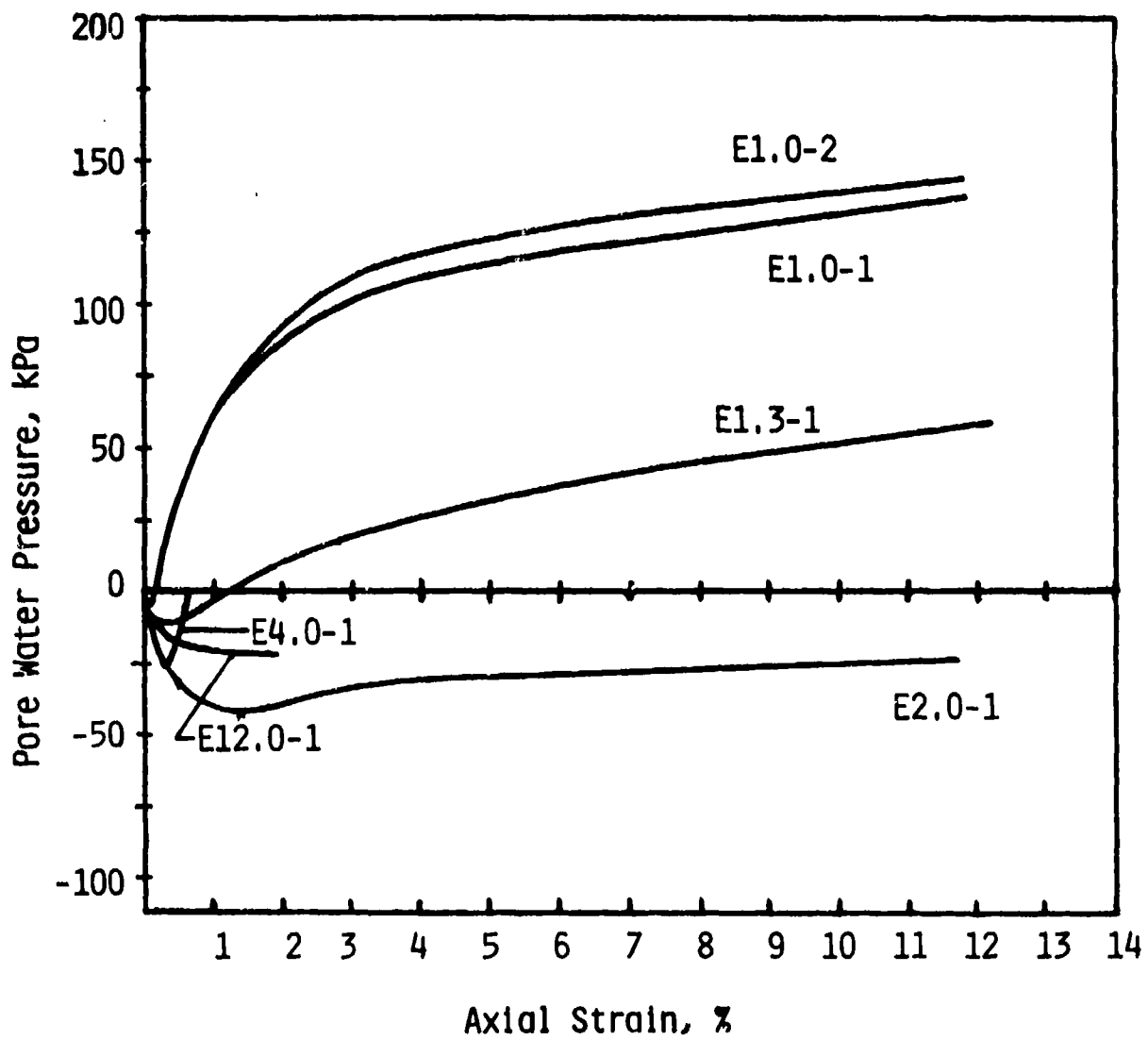


Figure 3.6b: Pore Water Pressure - Axial Strain Relationships For Extension Tests

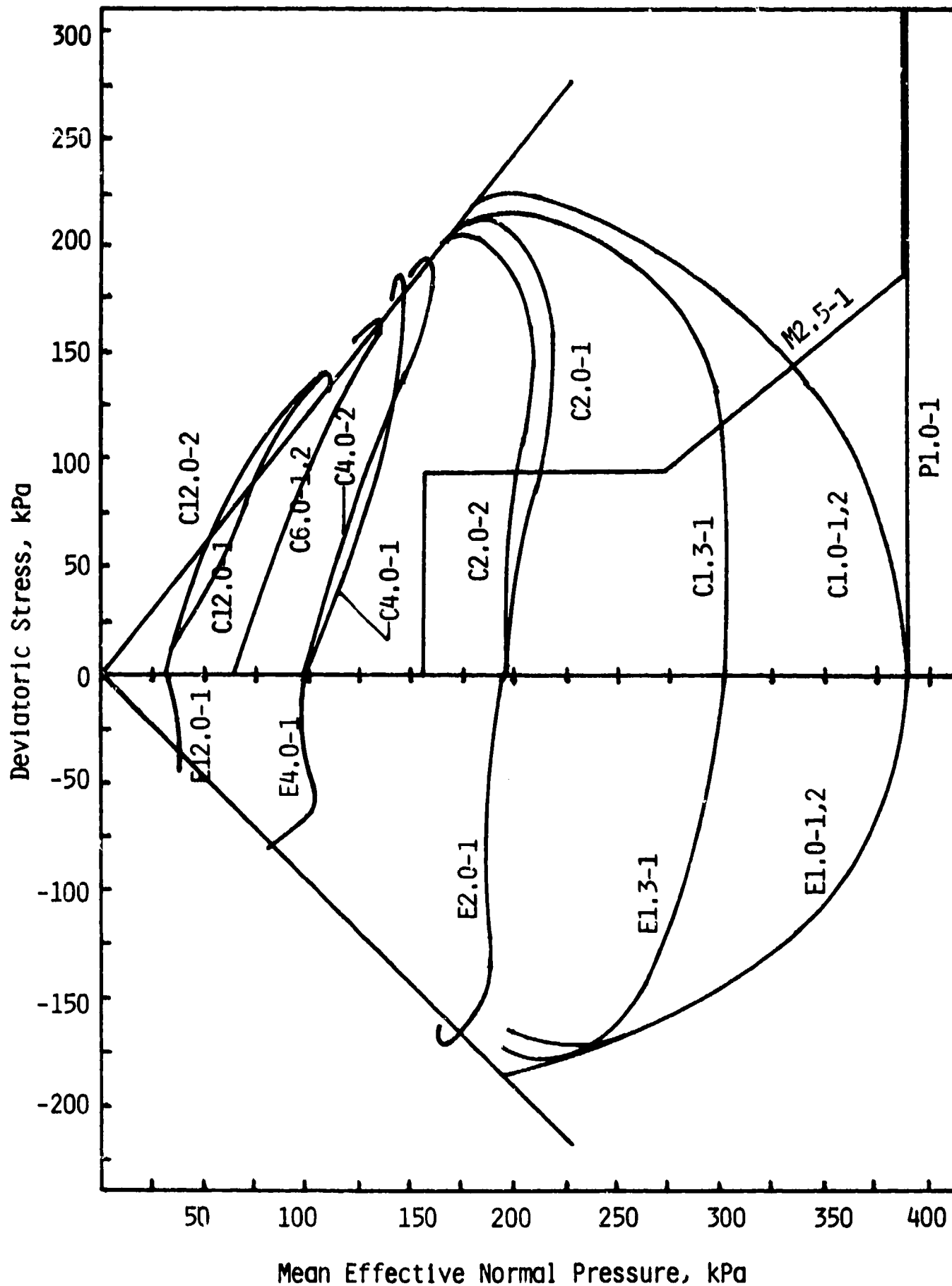


Figure 3.7: Stress Paths For Compression And Extension Tests

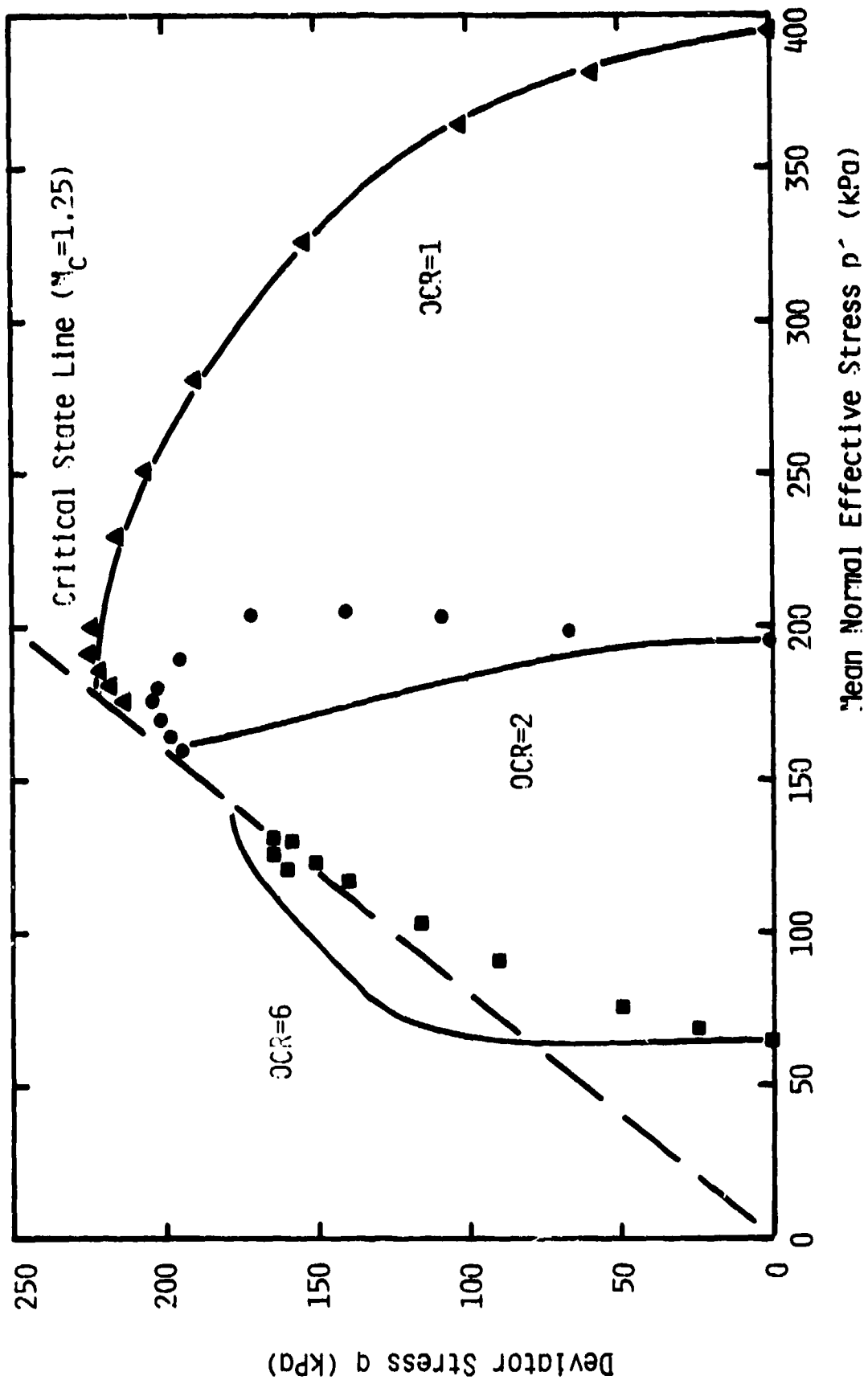


Figure 4.1: Calibration Curves for q vs. p' Relation in Triaxial Compression (projection point at origin)

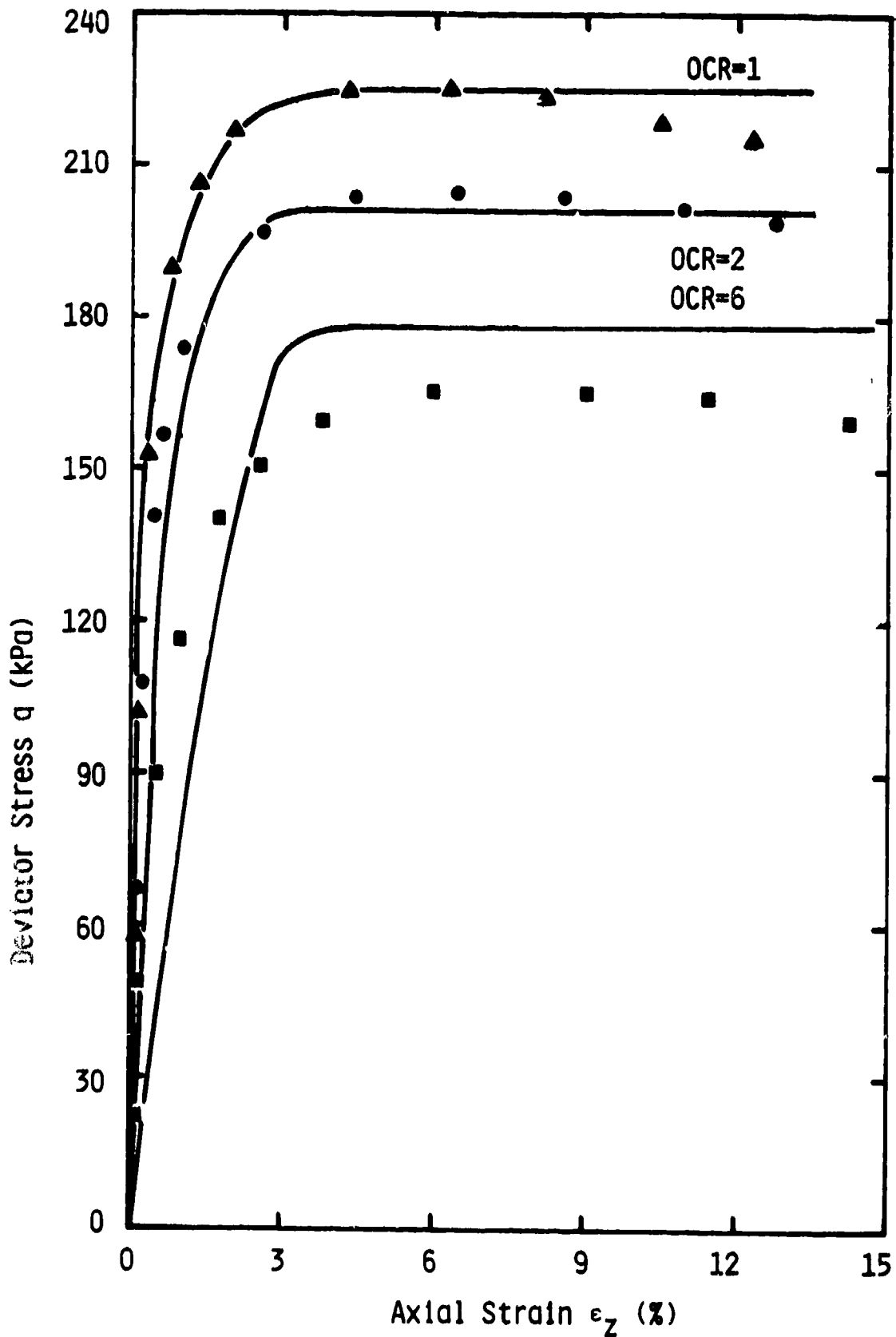


Figure 4.2: Calibration Curves for q vs. ϵ_z
 Relation in Triaxial Compression
 (Projection Point at Origin)

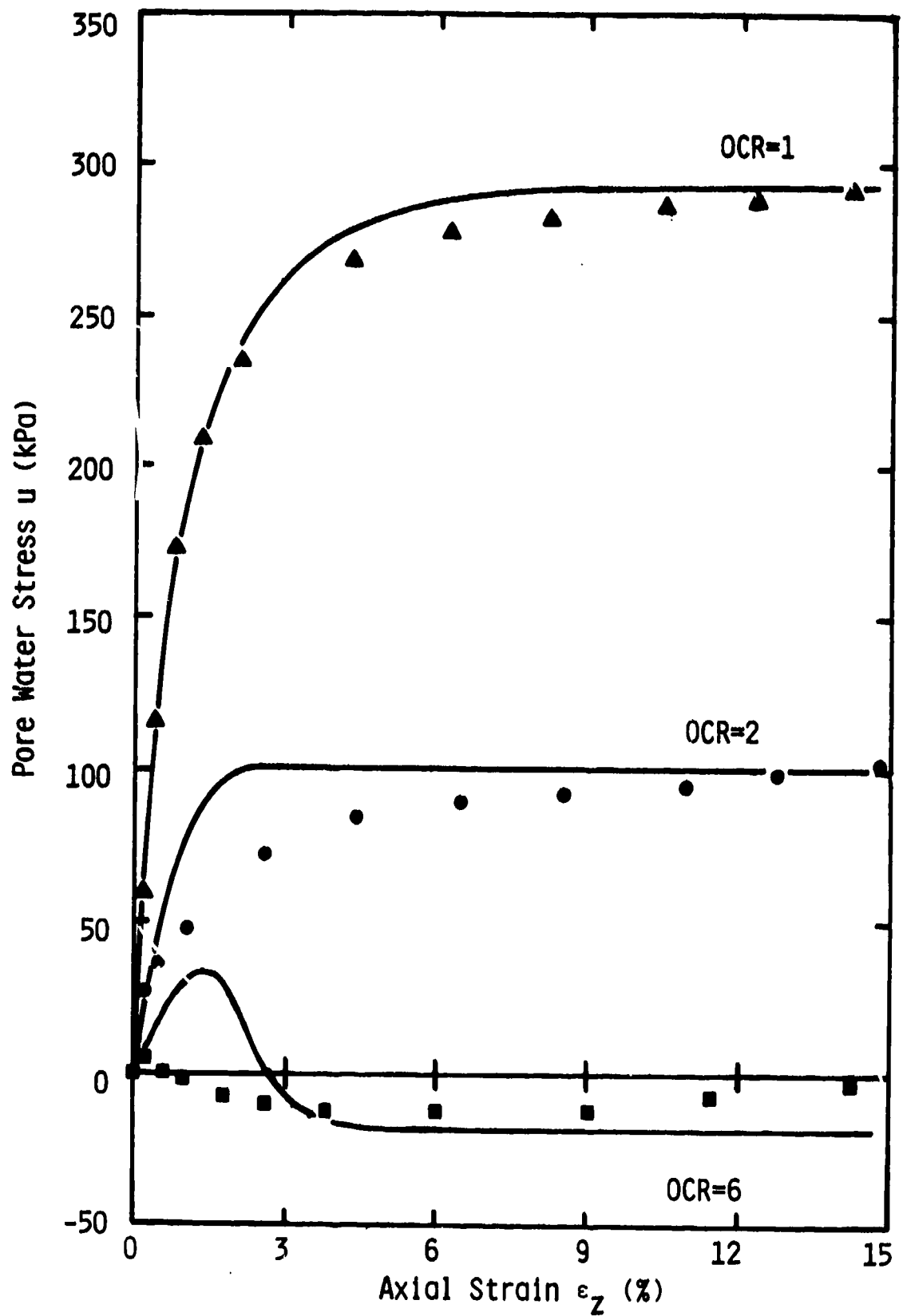


Figure 4.3: Calibration Curves for q vs. ϵ_z
 Relation in Triaxial Compression
 (Projection Point at Origin)

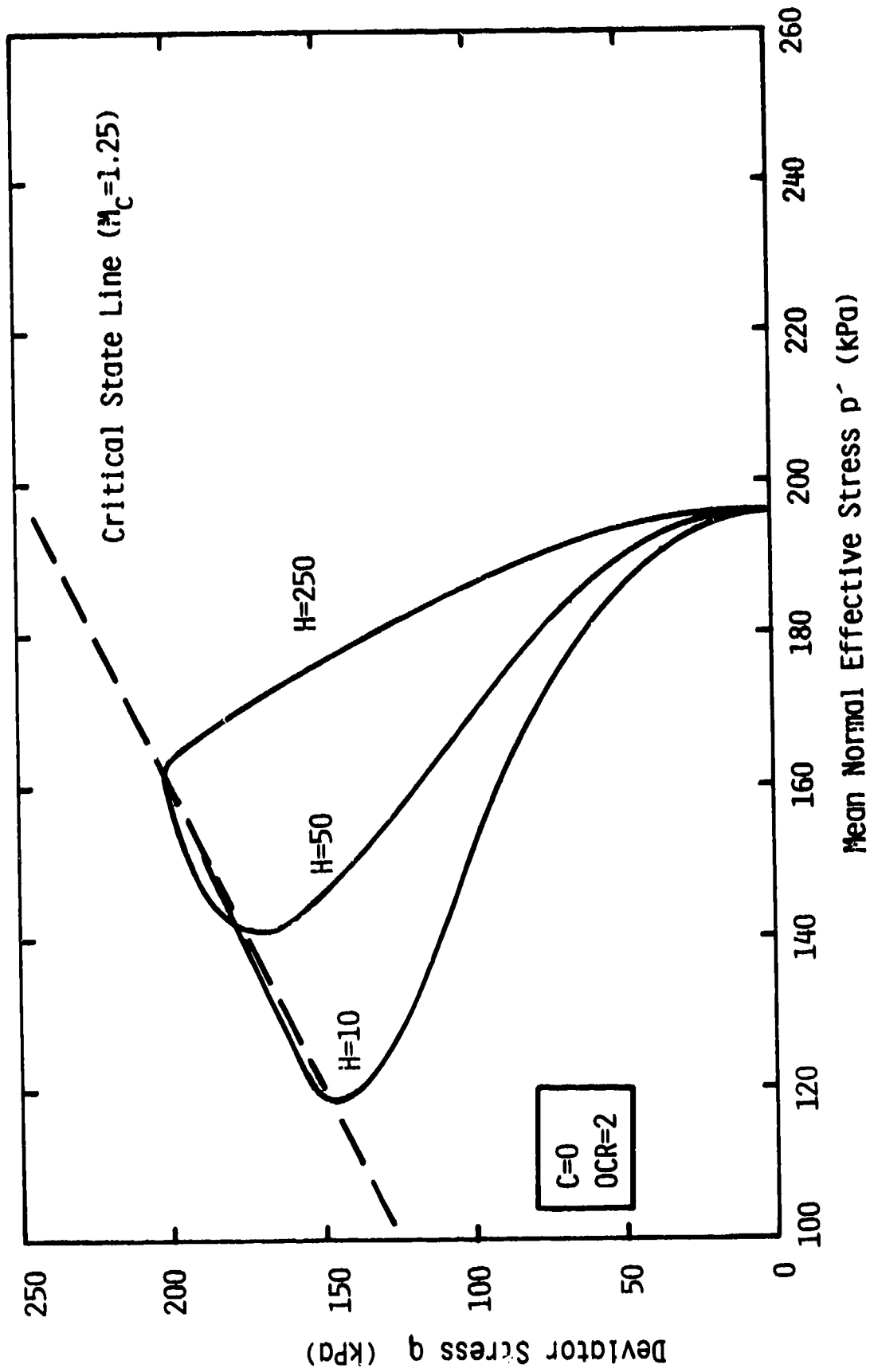


Figure 4.4: Influence of Hardening Parameter H_c on the Response of a Slightly Overconsolidated Clay

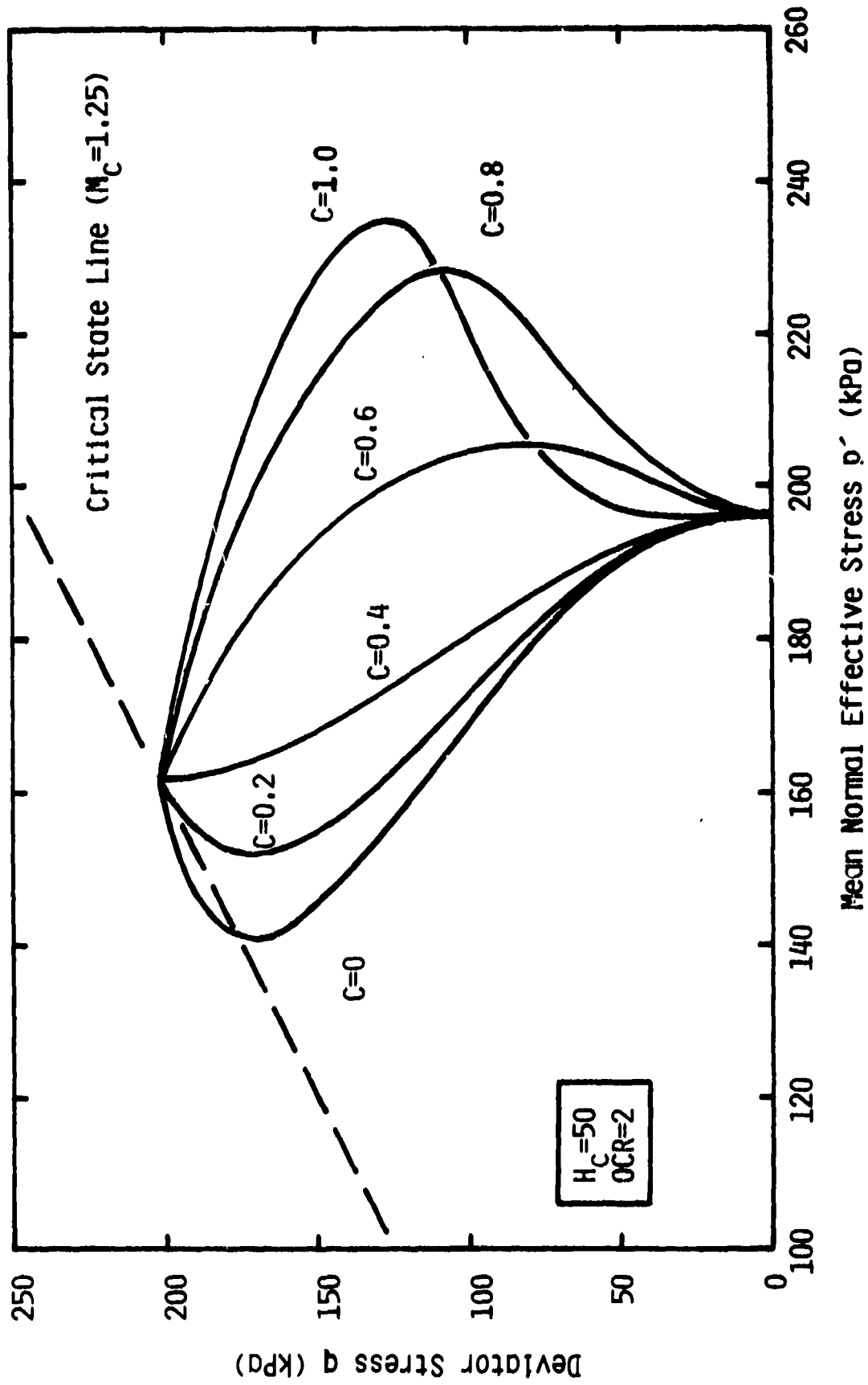


Figure 4.5: Influence of Projection Point Parameter c on the Response of a Slightly Overconsolidated Clay

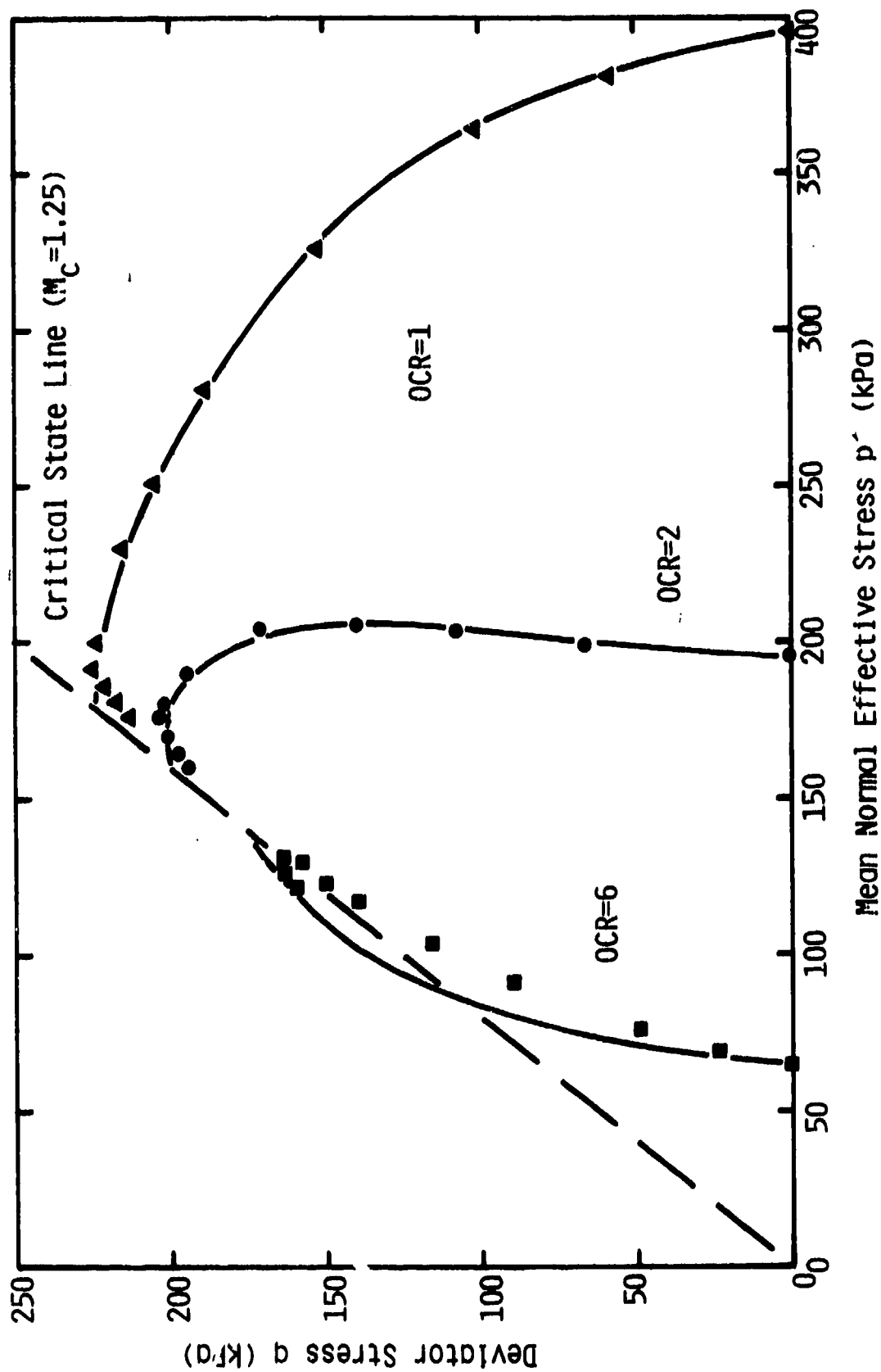


Figure 4.6: Calibration Curves for q vs. p' Relation in Triaxial Compression

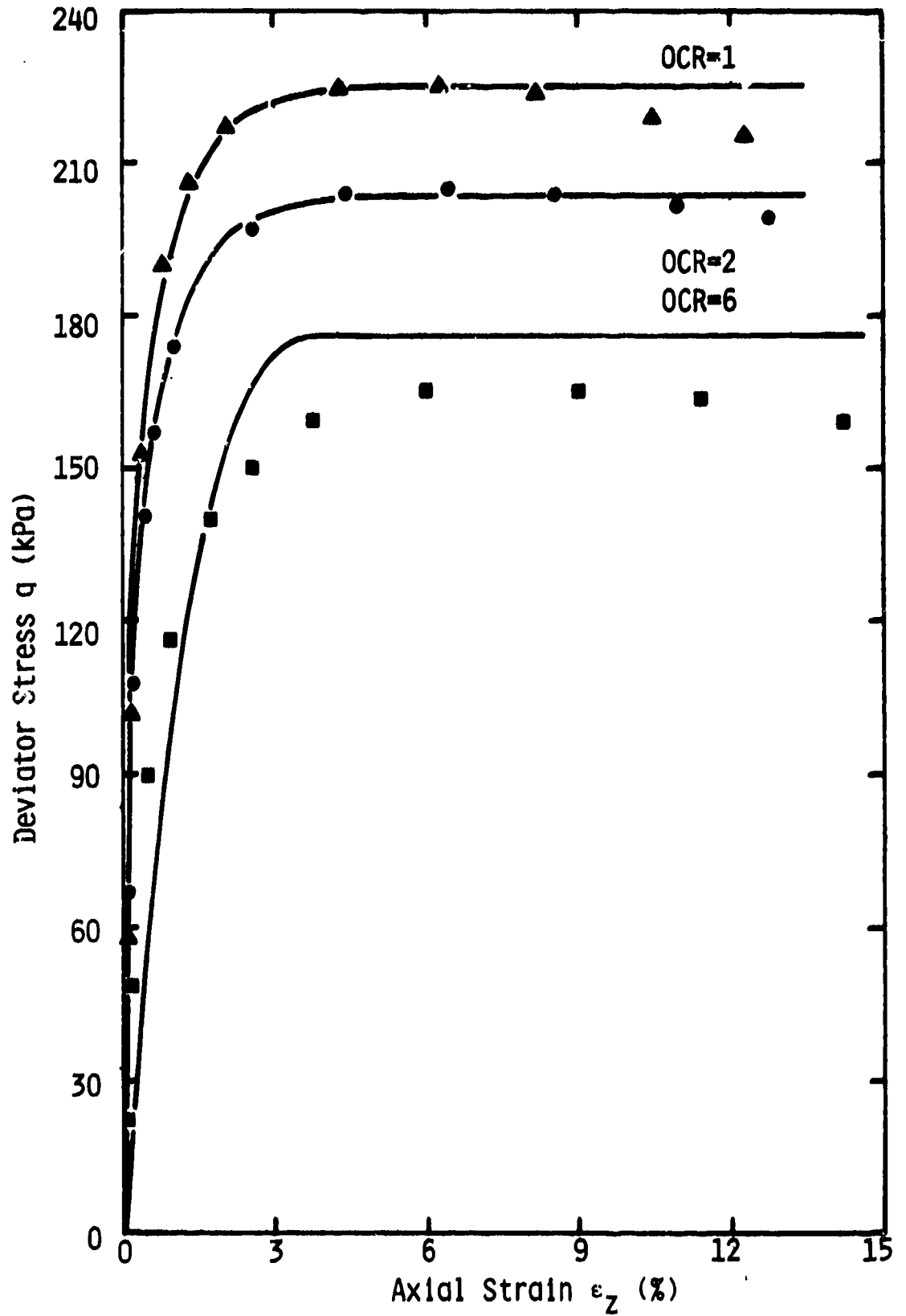


Figure 4.7: Calibration Curves for q vs. ϵ_z Relation in Triaxial Compression

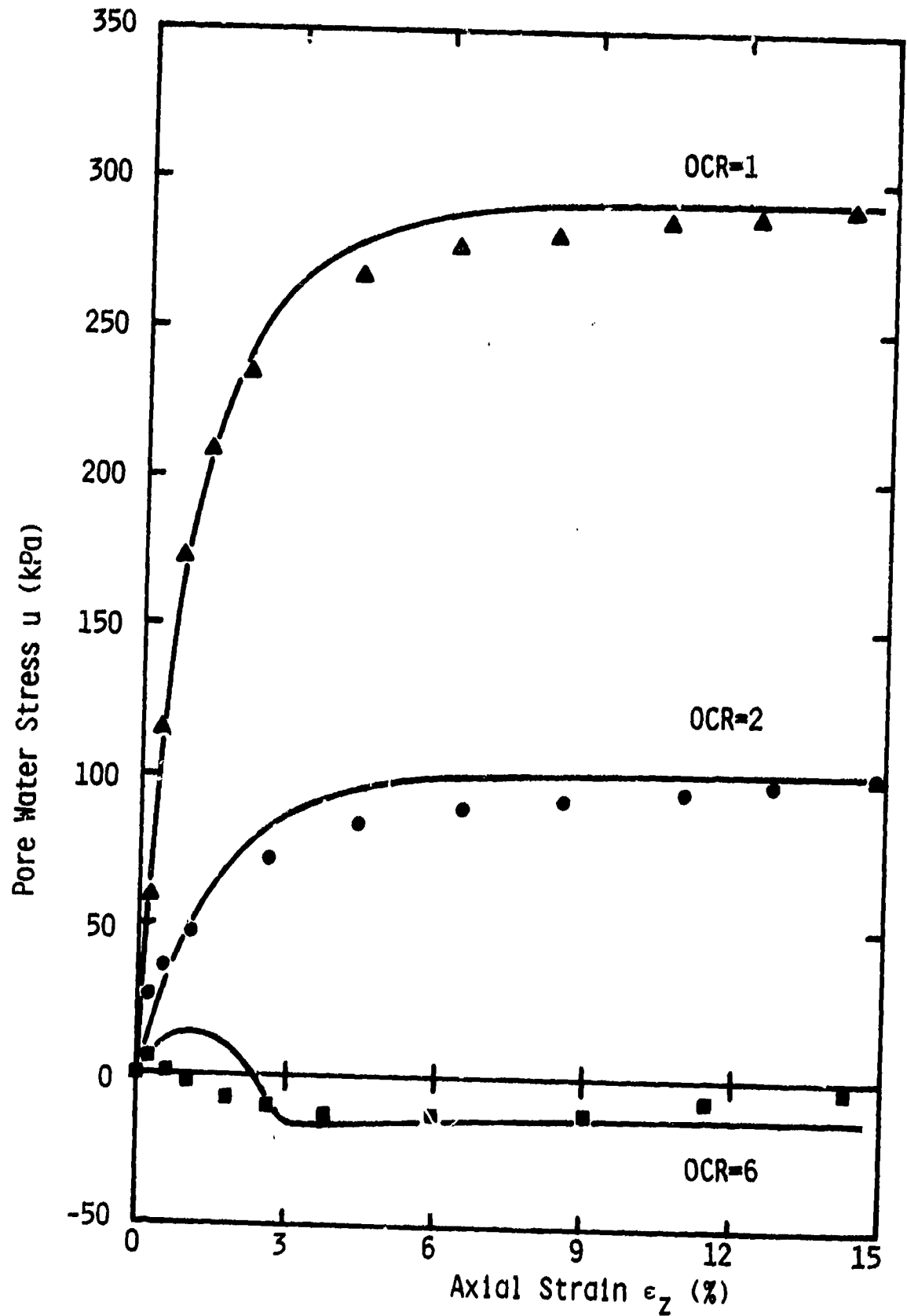


Figure 4.8: Calibration Curves for q vs. u Relation in Triaxial Compression

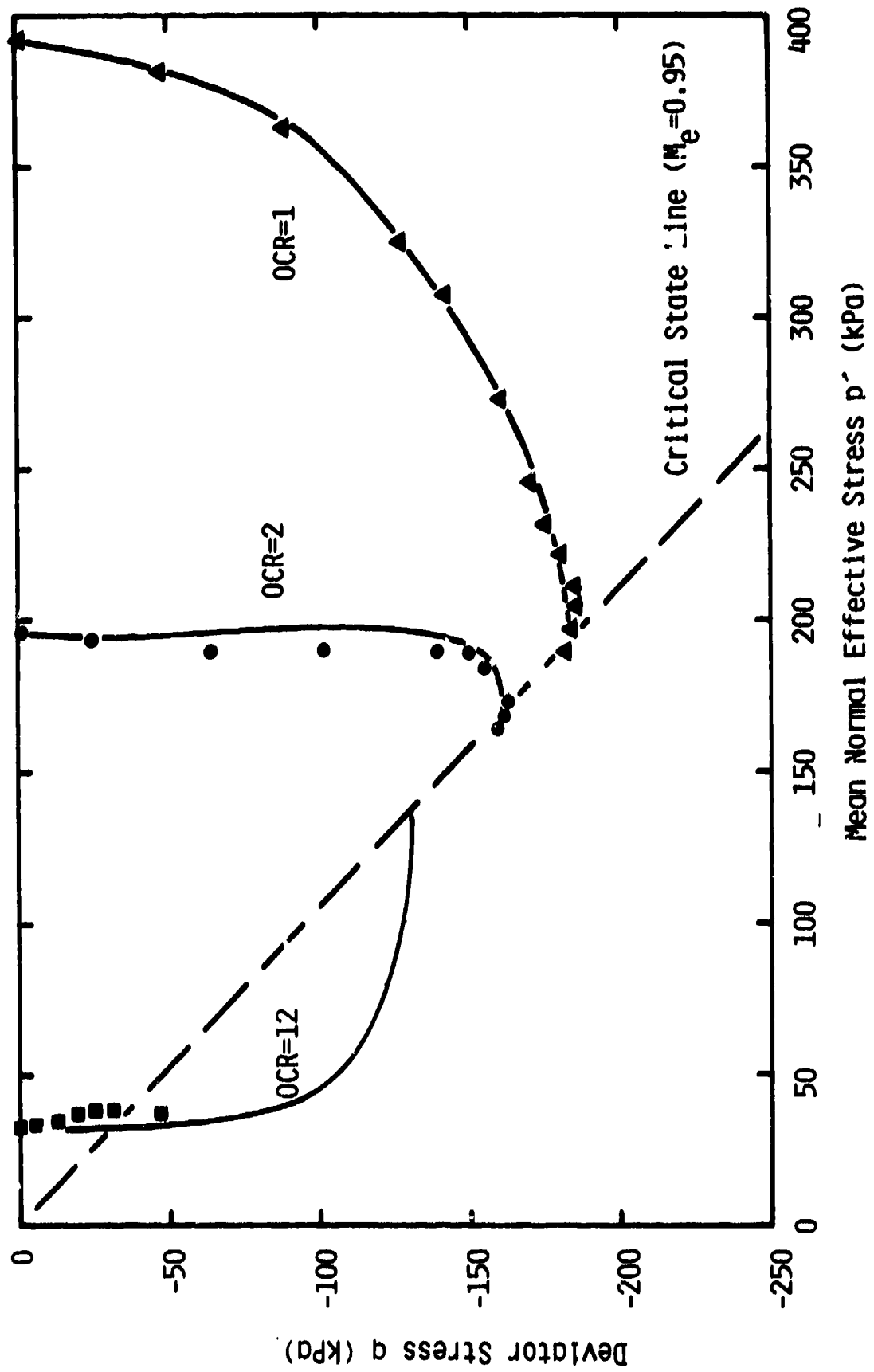


Figure 4.9: Calibration Curves for q vs. p' Relation in Triaxial Extension

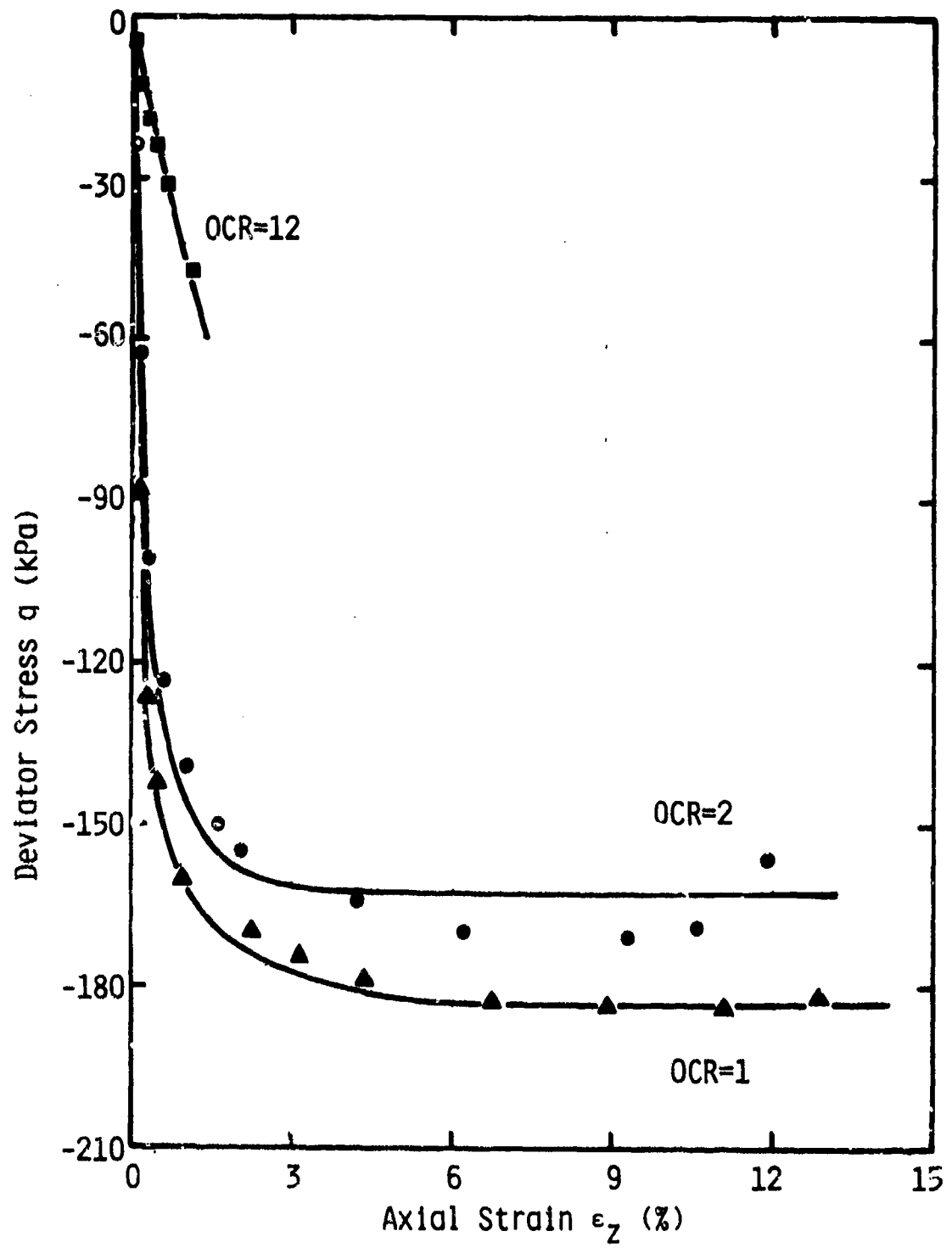


Figure 4.10: Calibration Curves for q vs. ϵ_z Relation in Triaxial Extension

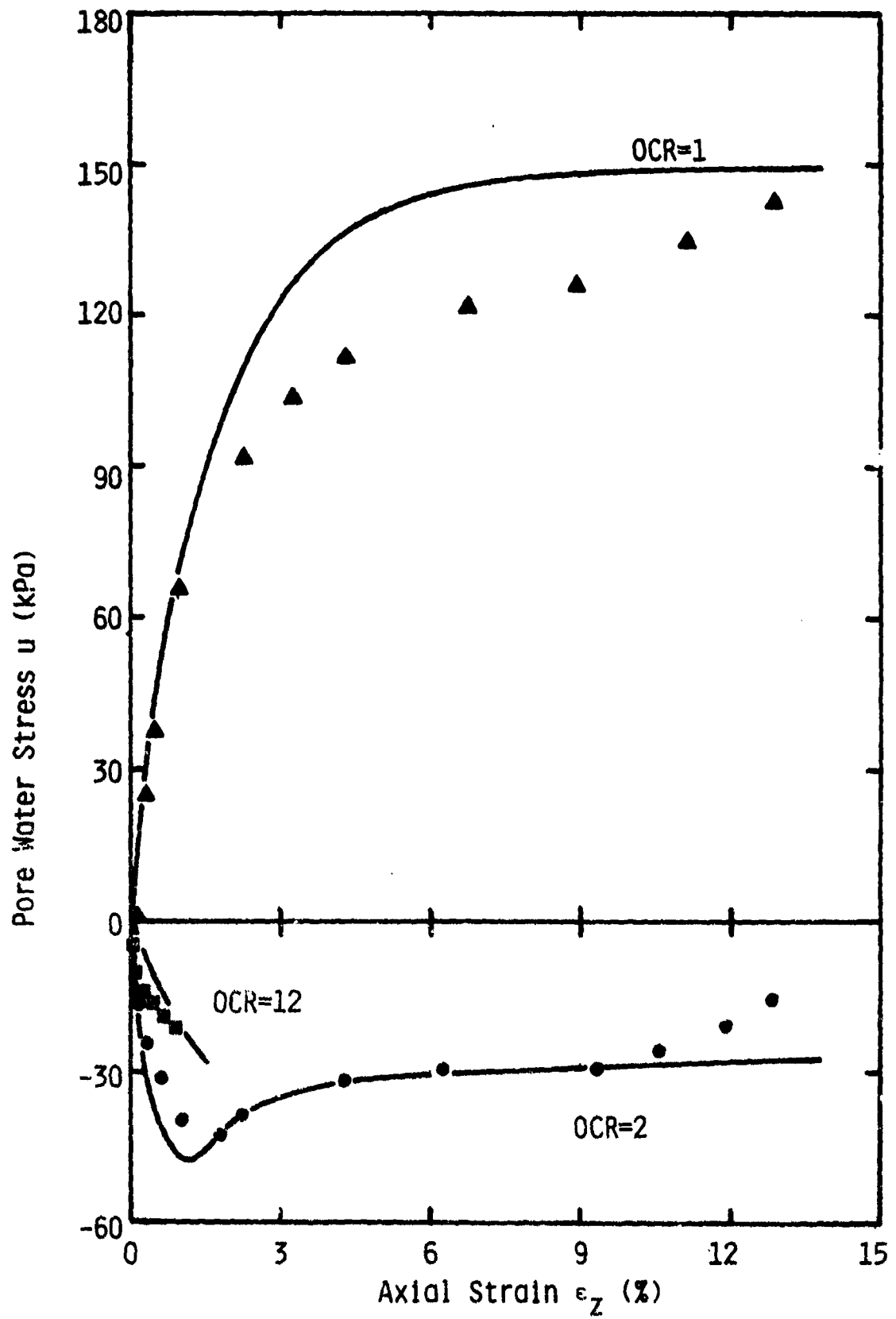


Figure 4.11: Calibration Curves for u vs. ϵ_z Relation in Triaxial Extension

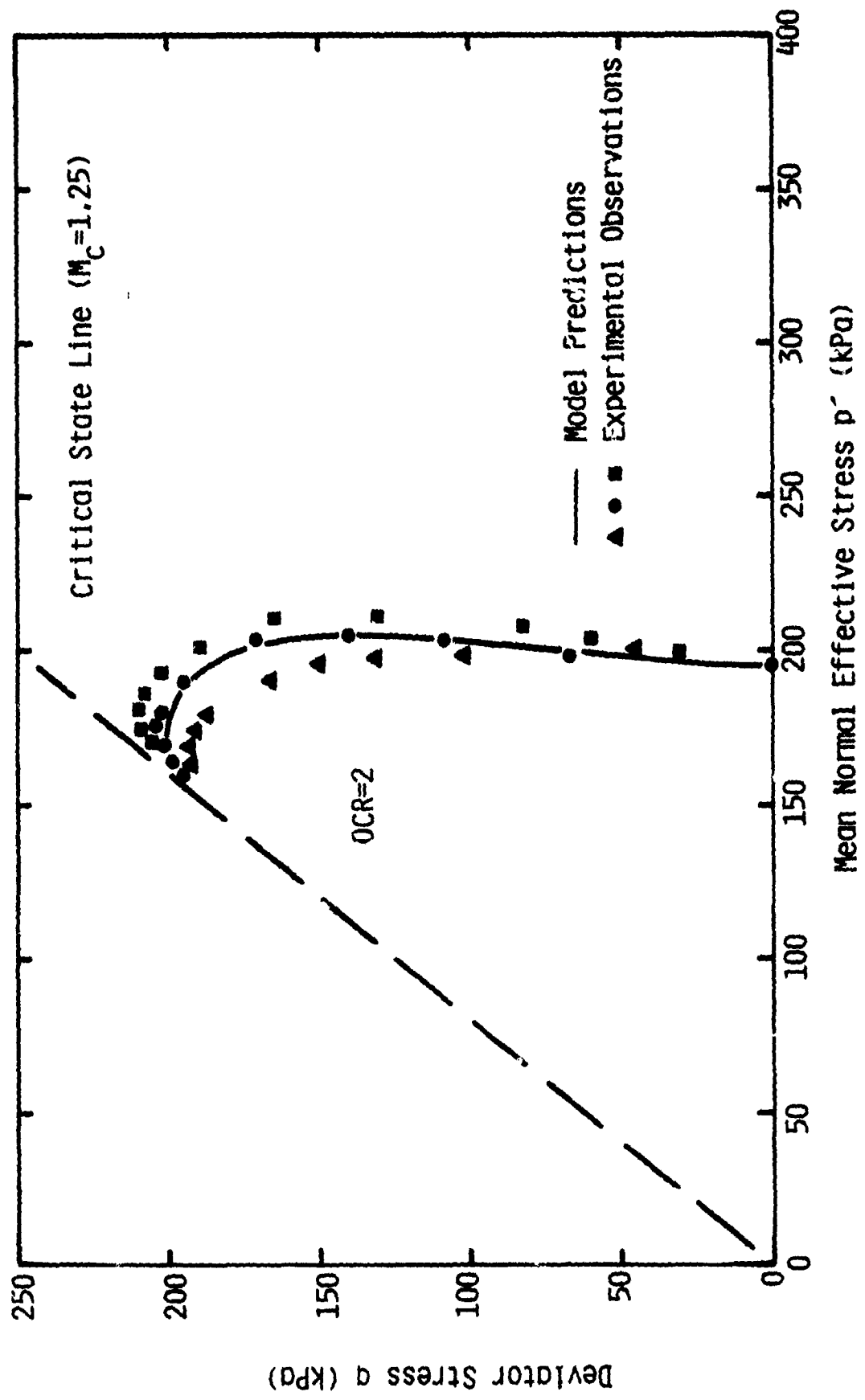


Figure 4.12: Model Predictions vs. Experimental Observations Showing Typical Scatter Band

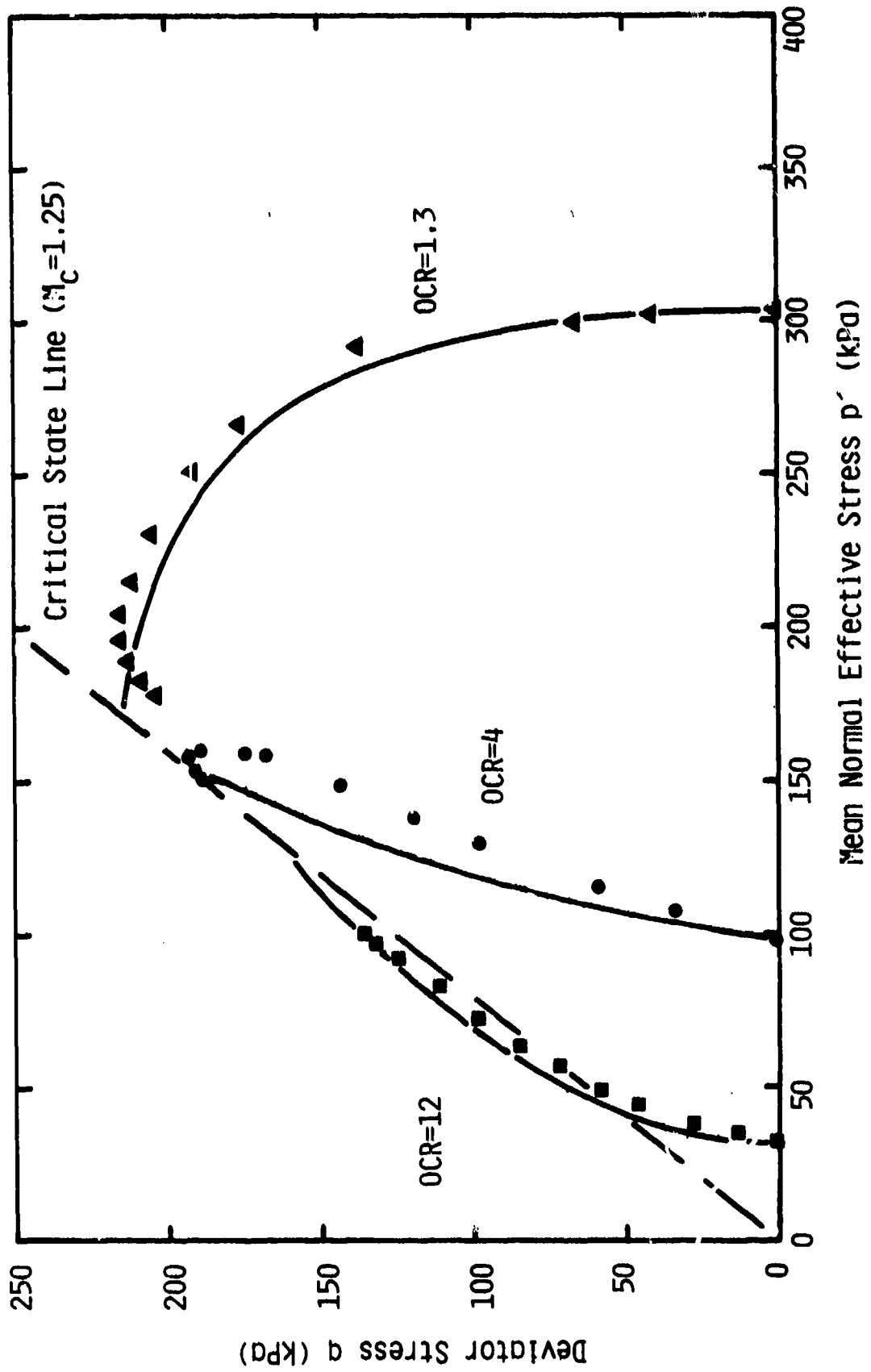


Figure 4.13: Prediction Curves for q vs. p' Relation in Triaxial Compression

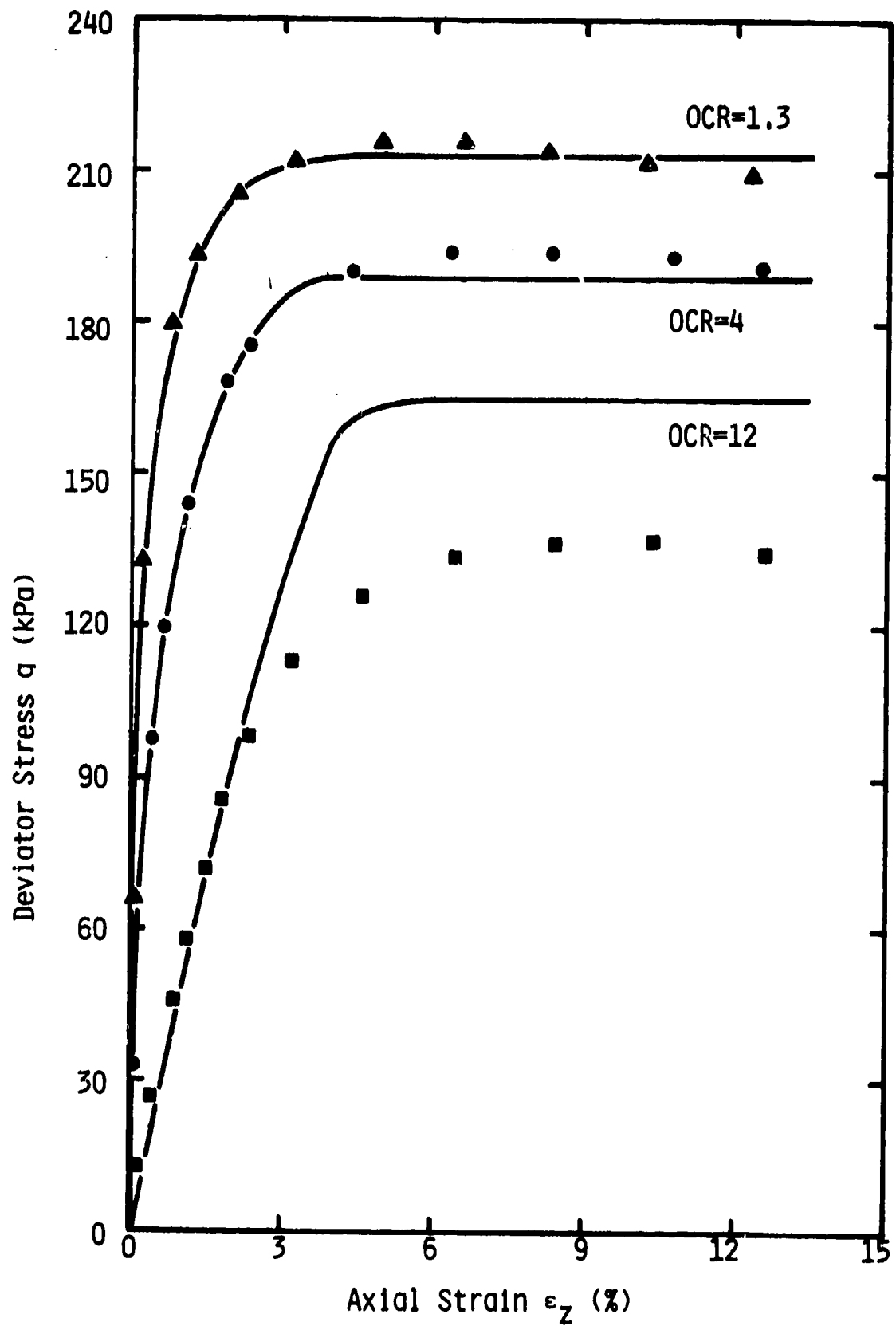


Figure 4.14: Prediction Curves for q vs. ϵ_z Relation in Triaxial Compression

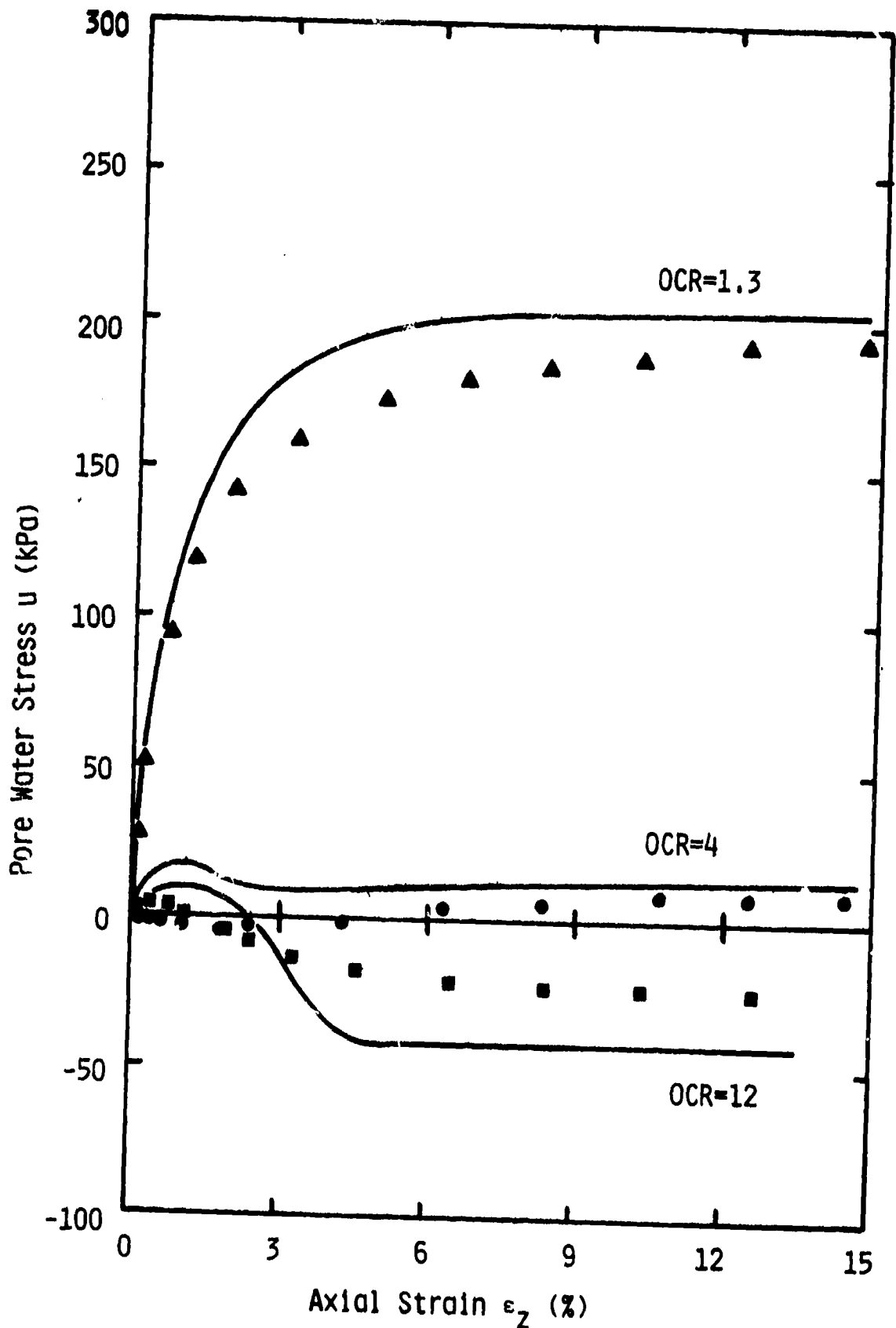


Figure 4.15: Prediction Curves for u vs. ϵ_z Relation in Triaxial Compression

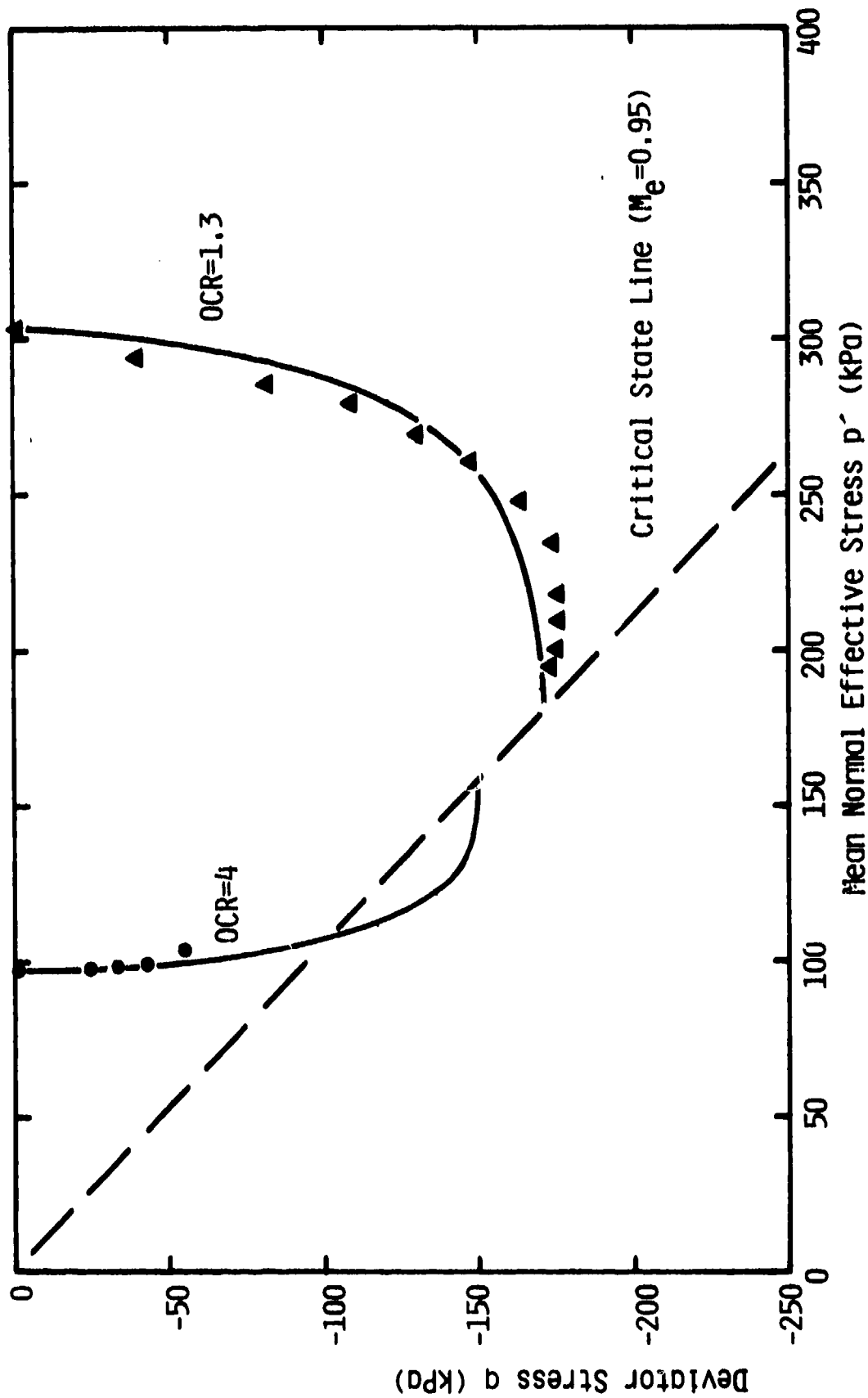


Figure 4.16: Prediction Curves for q vs. p' Relation in Triaxial Extension

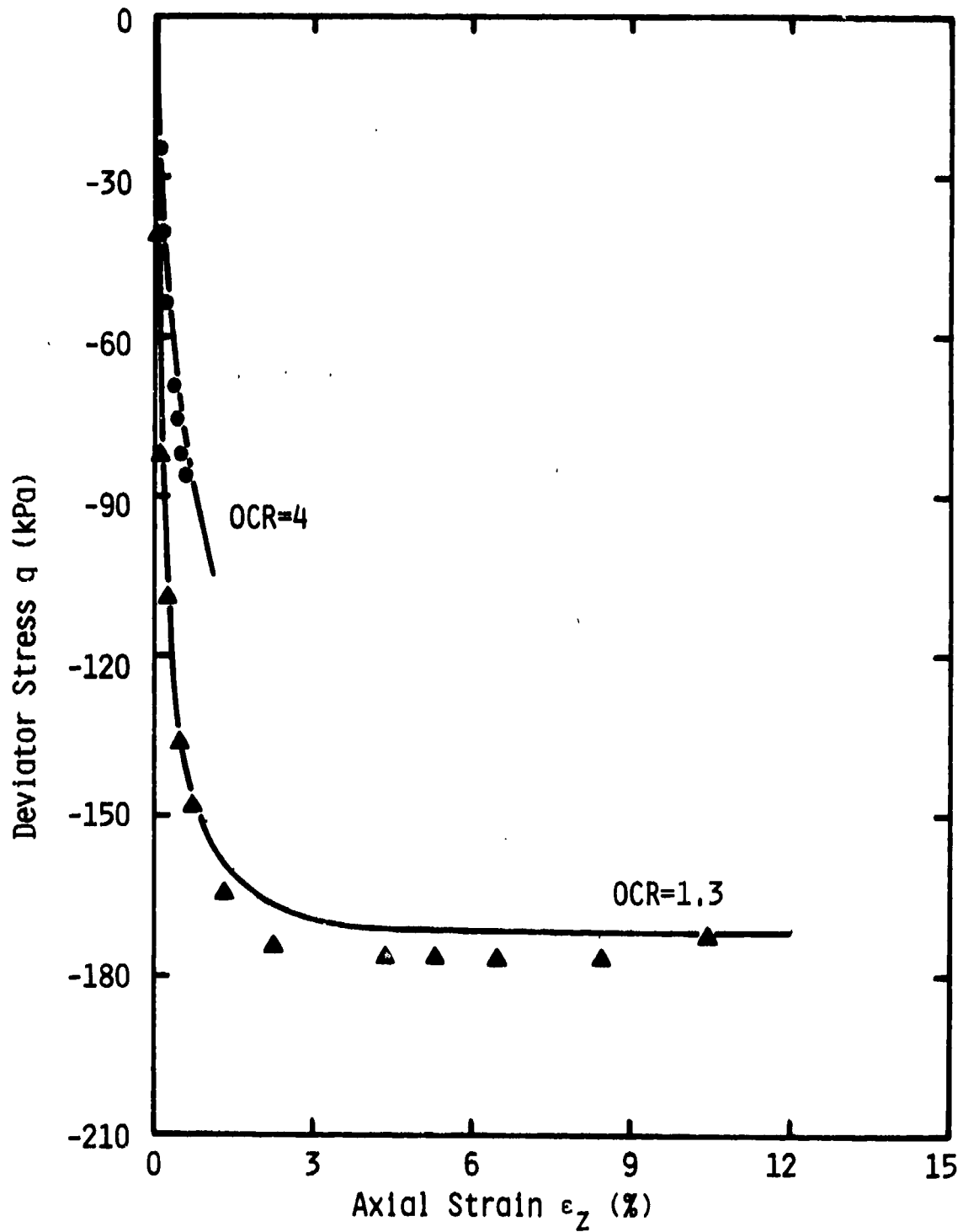


Figure 4.17: Prediction Curves for q vs. ϵ_z Relation in Triaxial Extension

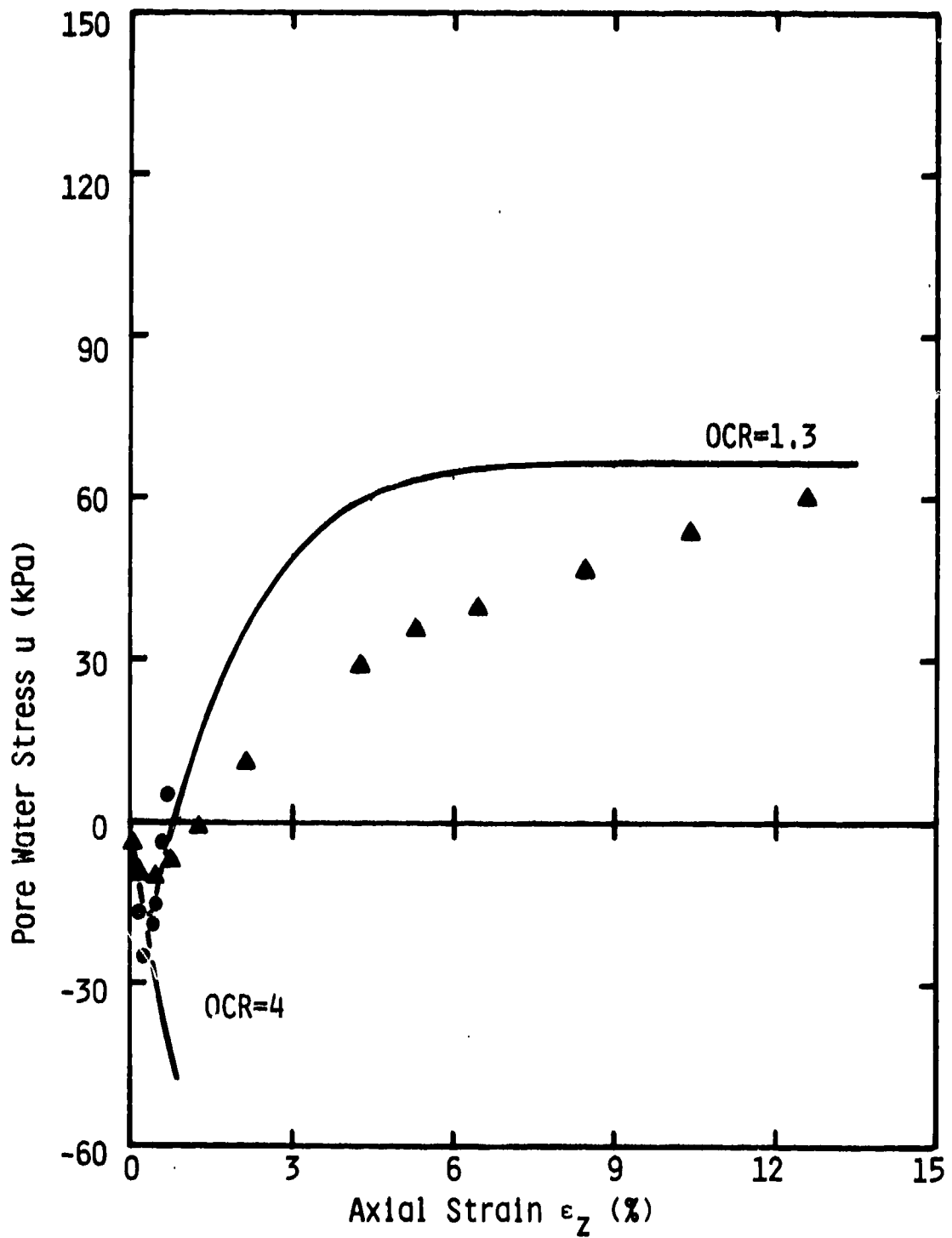


Figure 4.18: Prediction Curves for u vs. ϵ_z Relation in Triaxial Extension

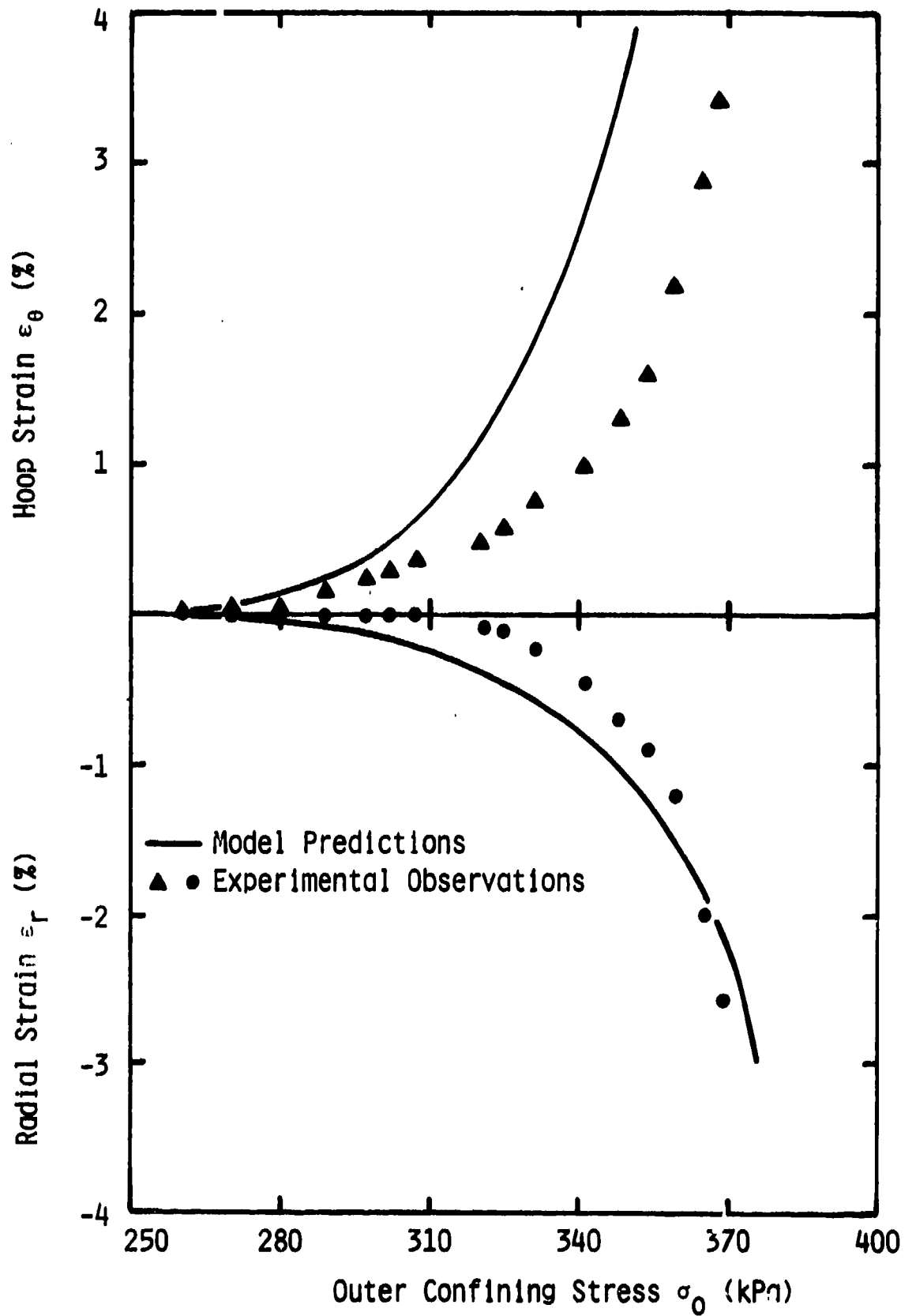


Figure 4.19: Predictions for ϵ_θ and ϵ_r vs. σ_o -
Hollow Cylinder Test #1 Assuming
Homogeneous Stress and Strain

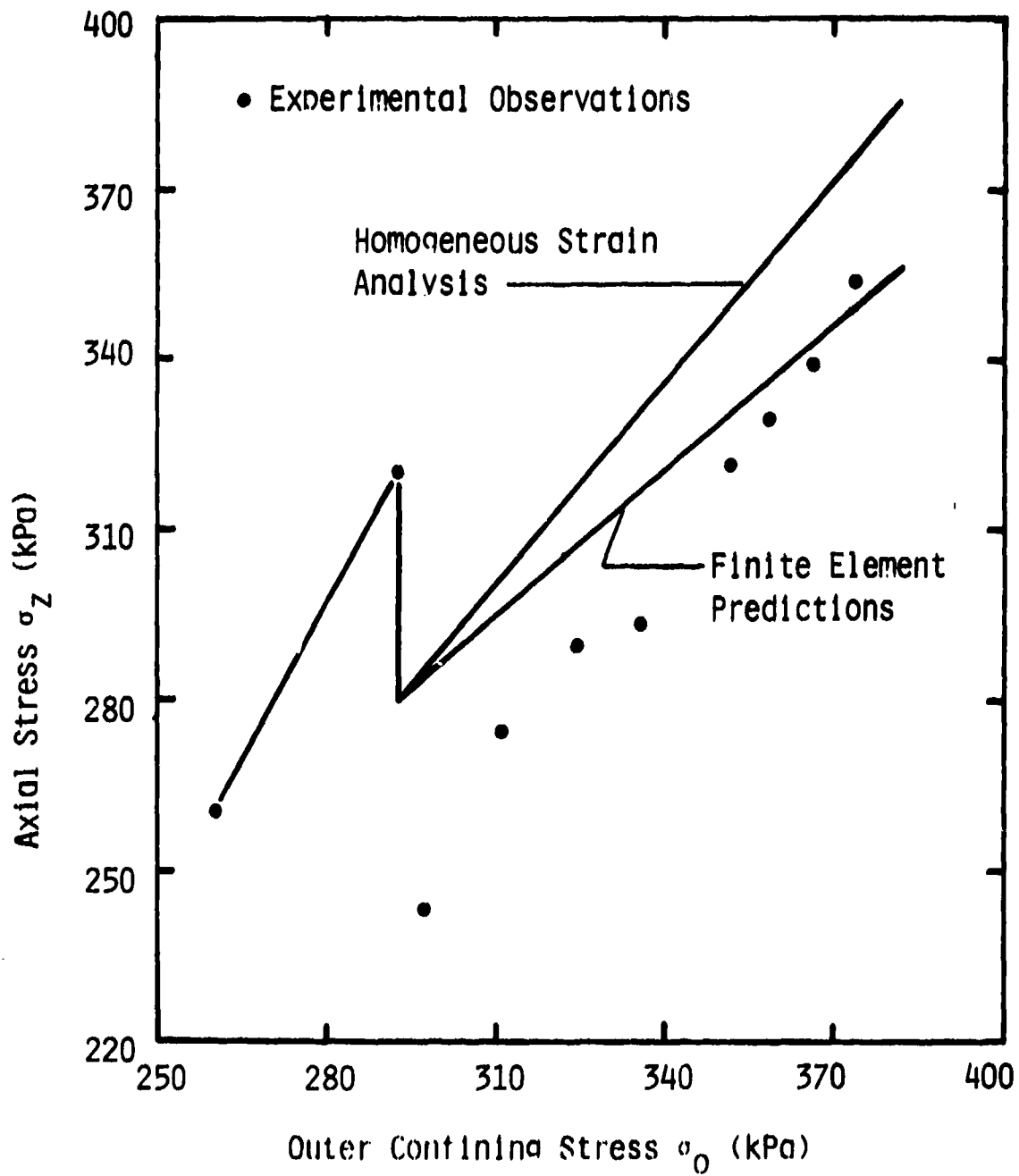


Figure 4.20: Prediction Curves For σ_z vs σ_0 --
Hollow Cylinder Test #1

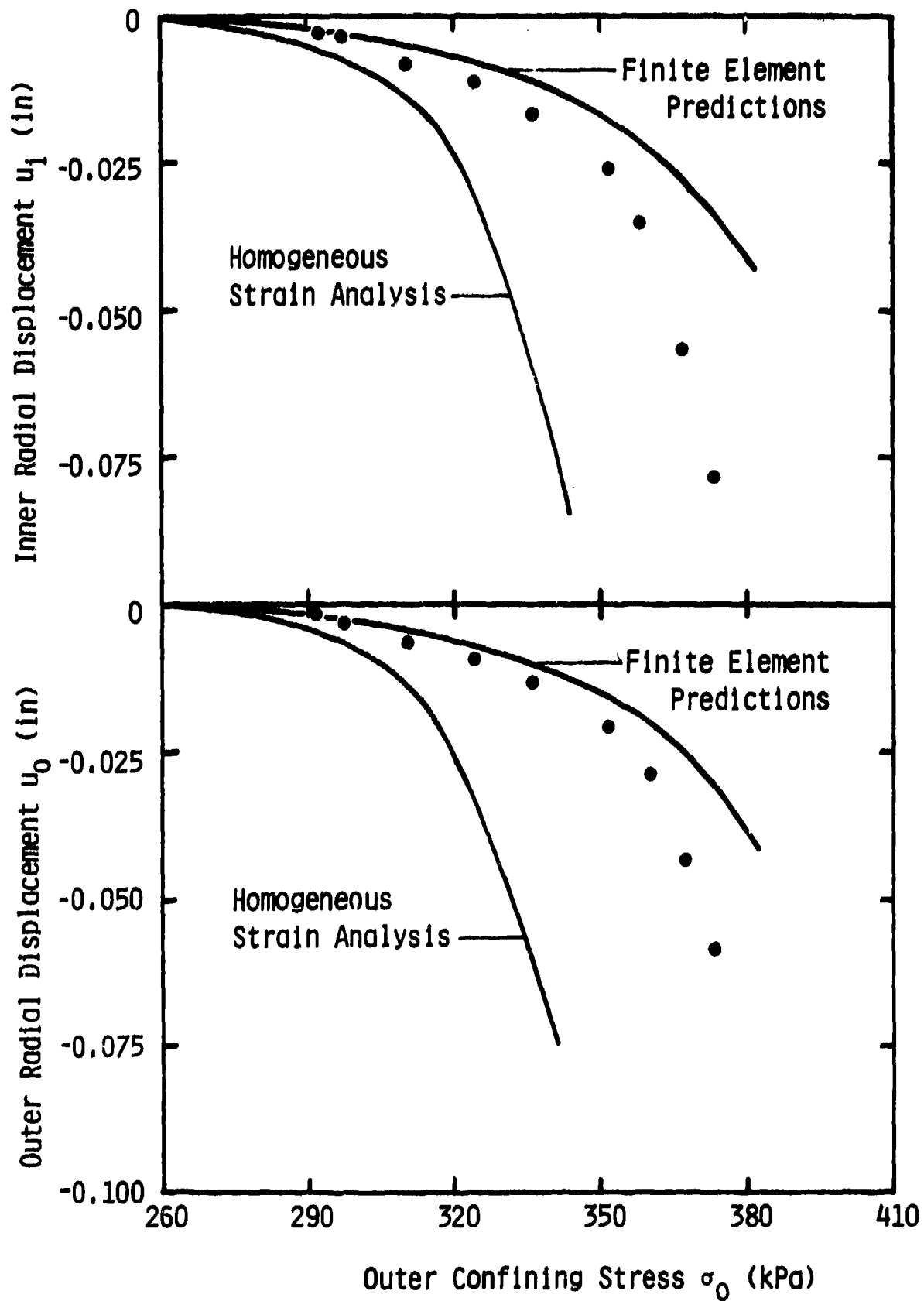


Figure 4.21: Prediction Curves For u_1 and u_0 vs σ_0 -- Hollow Cylinder Test #1

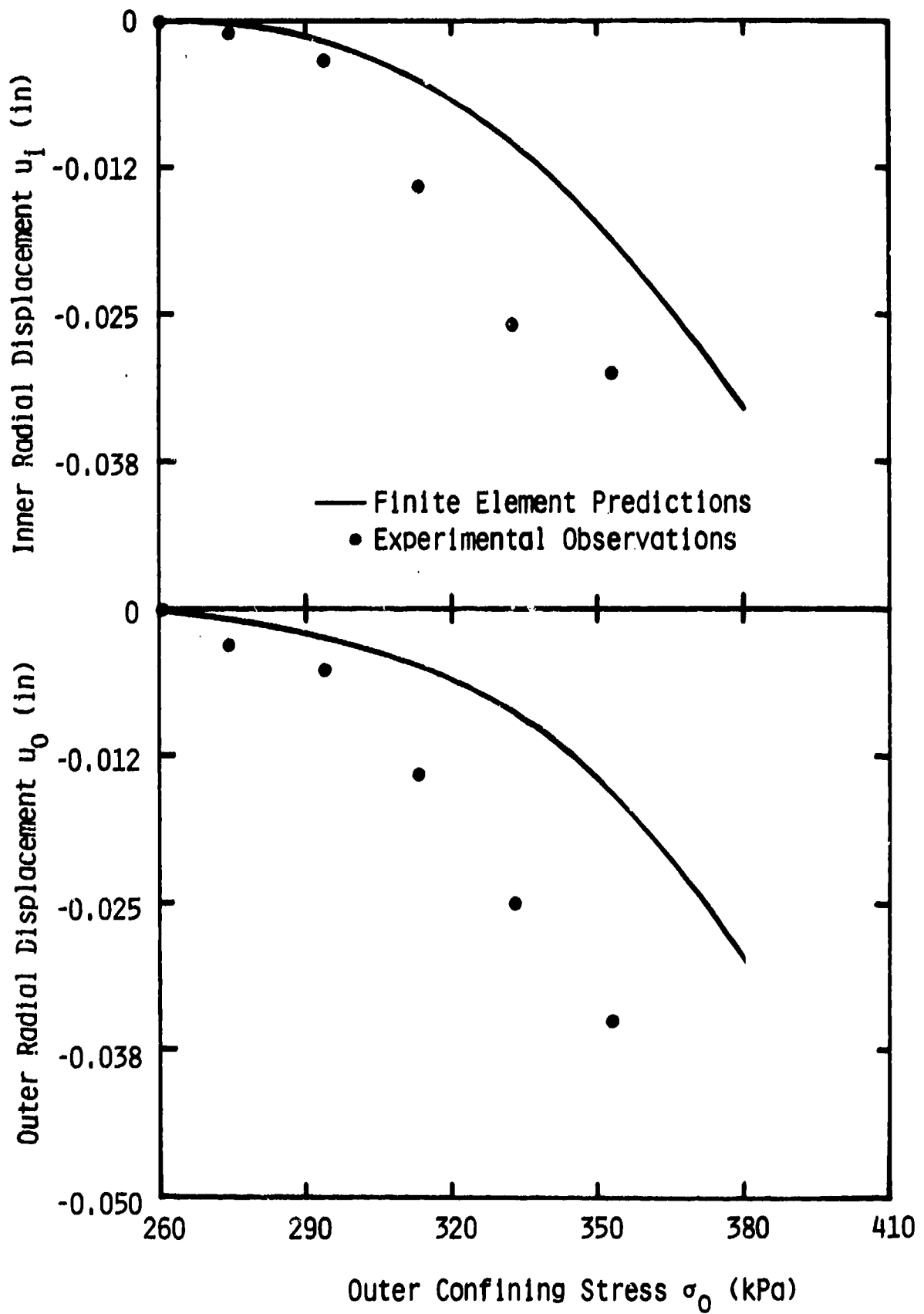
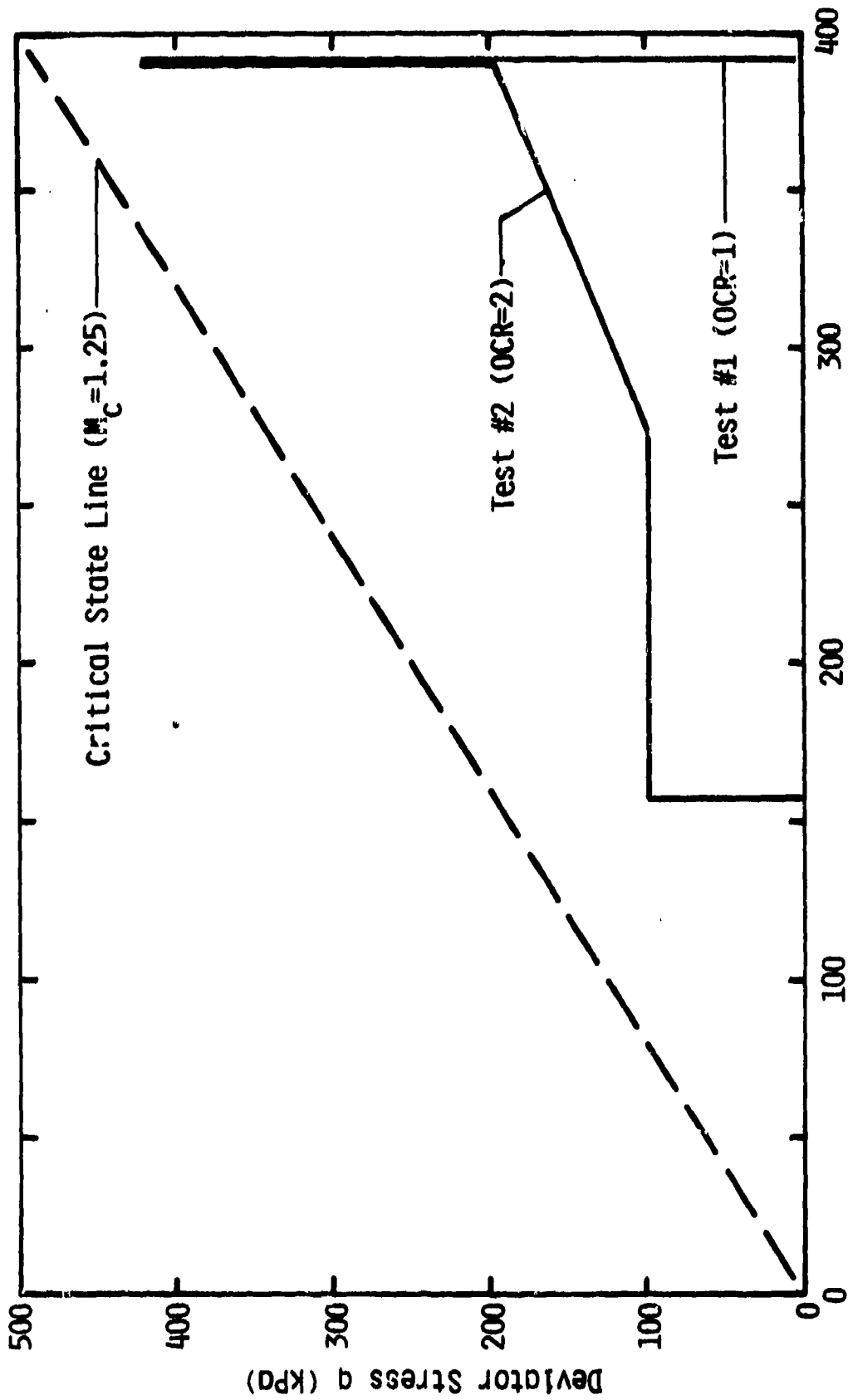


Figure 4.22: Prediction Curves For u_i and u_o vs σ_0 -- Hollow Cylinder Test #2



Mean Normal Effective Stress p' (kPa)

Figure 4.23: Stress Paths - Drained Triaxial Compression Tests #1 and #2

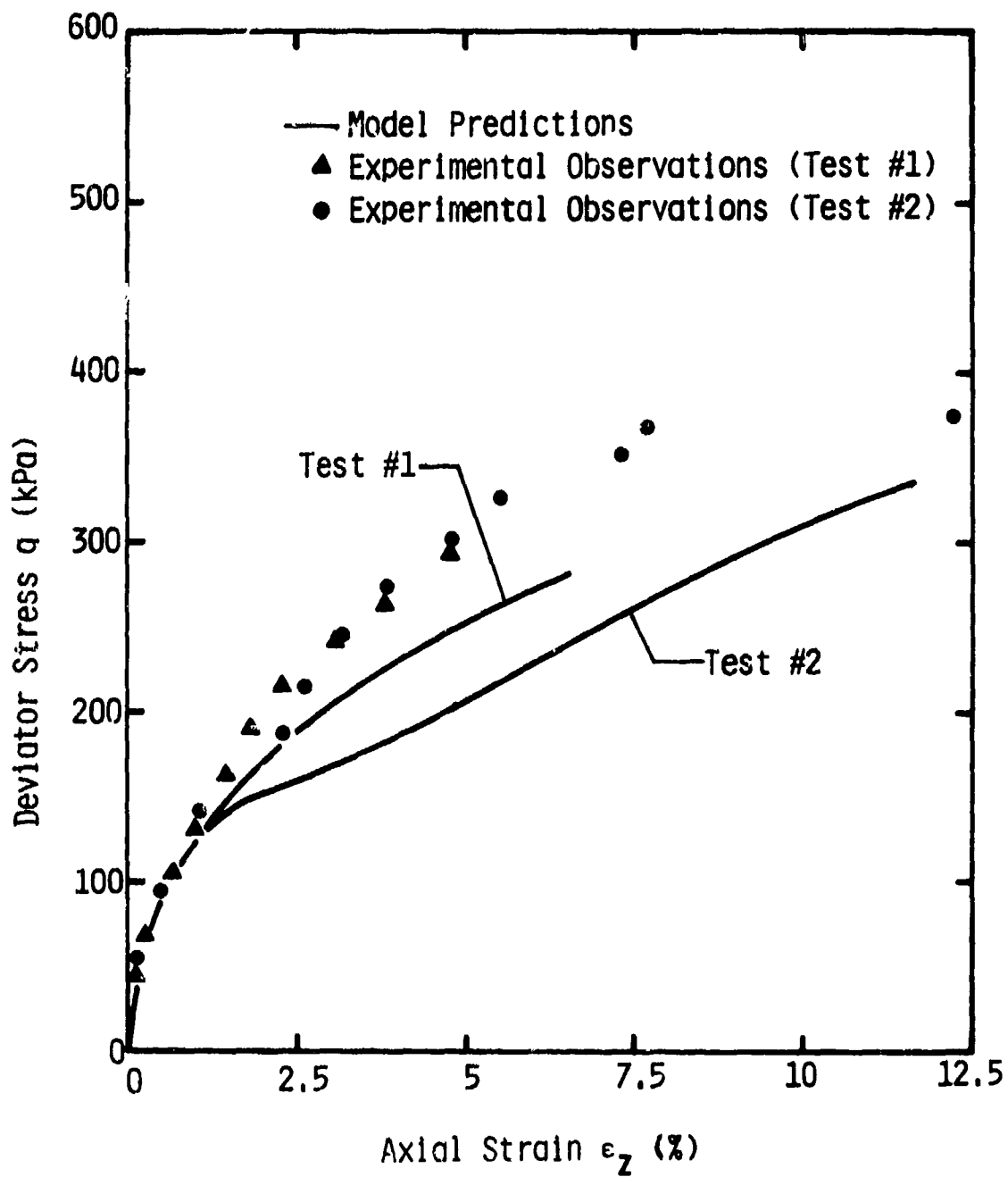


Figure 4.24a: Prediction Curves for q vs ϵ_z --
 Drained Triaxial Compression Tests #1 and #2

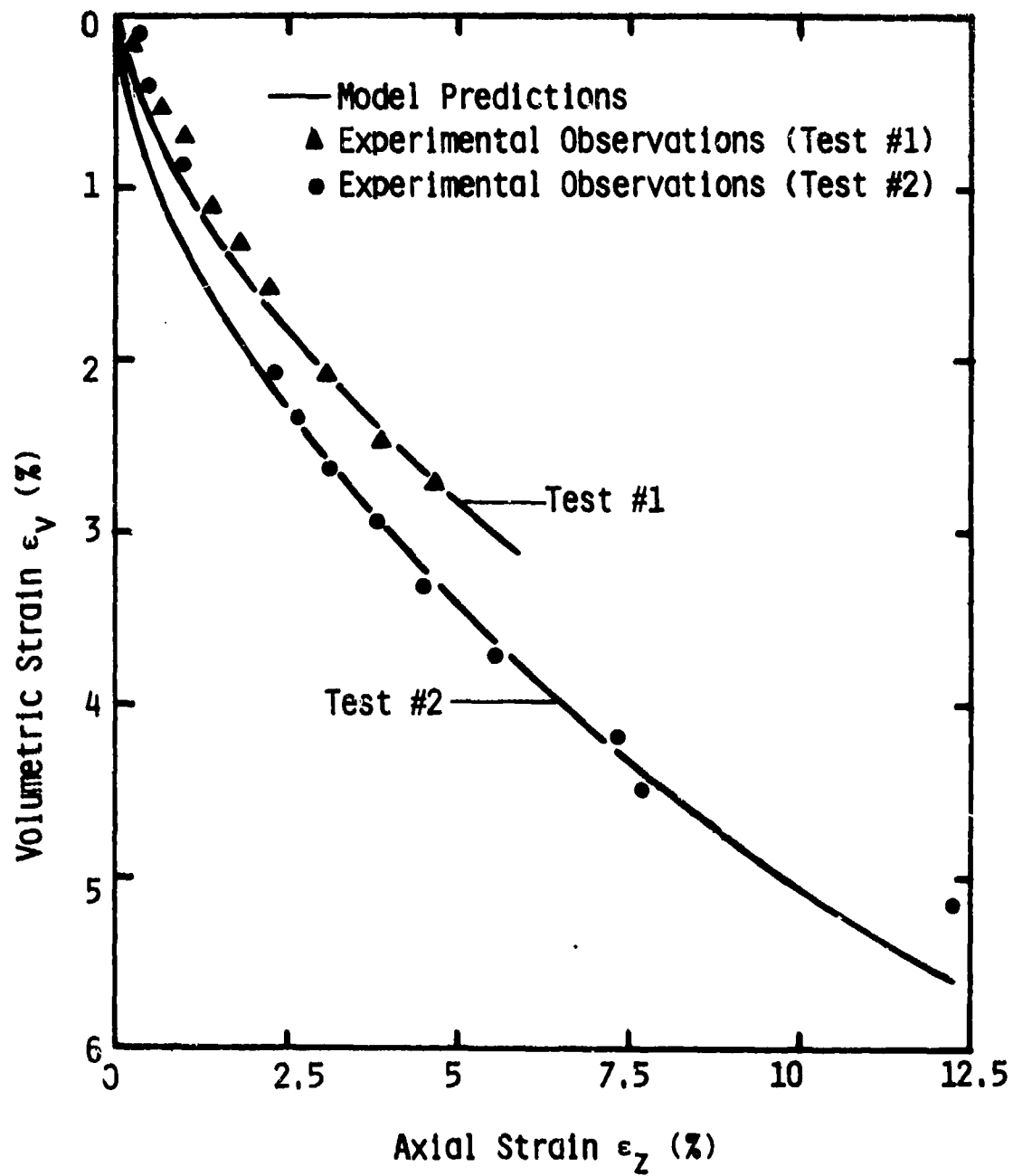


Figure 4.24b: Prediction Curves For ϵ_v vs ϵ_z --
 Drained Triaxial Compression
 Tests #1 and #2